Eur. Phys. J. A **2**, 199–221 (1998)

THE EUROPEAN PHYSICAL JOURNAL A

Low- and intermediate-energy nucleon-nucleon interactions and the analysis of deuteron photodisintegration within the dispersion relation technique

A.V. Anisovich, V.A. Sadovnikova

Petersburg Nuclear Physics Institute, Gatchina, St.Petersburg 188350, Russia

Received: 24 November 1997
Communicated by B. Povh

Abstract. Nucleon-nucleon interactions in the region of the nucleon kinetic energies up to 1000 MeV are analysed together with the reaction $\gamma d \to pn$ in the photon energy range up to $E_\gamma = 400$ MeV. The following nucleon-nucleon s-channel partial amplitudes are reconstructed in the dispersion relation N/D method: $^1S_0$, $^3S_1 - ^3D_1$, $^3P_0$, $^1P_1$, $^3P_1$, $^3P_2$, $^1D_2$, $^3D_2$ and $^3F_3$. Correspondingly, the dispersive representation of partial amplitudes $N\Delta \to pn$, $NN^* \to pn$ and $NN\pi \to pn$ is given and parameters which determine these two baryon amplitudes are found. Basing on that, we have performed parameter-free calculation of the amplitude $\gamma d \to pn$, taking into account: (i) pole diagram, (ii) nucleon-nucleon final-state rescattering $\gamma d \to pn \to pn$, and (iii) inelastic final-state rescatterings $\gamma d \to N\Delta(1232) \to pn$, $\gamma d \to NN^*(1400) \to pn$ and $\gamma d \to NN\pi \to pn$. The $\gamma d \to pn$ partial amplitudes for the above-mentioned channels are found. It is shown that the process $\gamma d \to pn \to pn$ is significant for the waves $^1S_0$, $^3P_0$, $^3P_1$, at $E_\gamma = 50 - 100$ MeV, while $\gamma d \to N\Delta \to pn$ dominates for the waves $^3P_2$, $^1D_2$, $^3F_3$ at $E_\gamma > 300$ MeV. Meson exchange current contributions into the deuteron disintegration are estimated: they are significant at $E_\gamma = 100 - 400$ MeV.

1 Introduction

Investigations of the lightest nuclei such as deuteron, ^3He, ^3H, or ^4He were always challenging for researchers. There are at least two reasons for that:

(i) Investigations of simple nuclei give a chance to comprehend better the crucial problems of nuclear physics, such as the structure of nucleon-nucleon forces, the role of multinucleon interactions, the role of internuclear forces at small and large distances, the problem of multiquark bags like $6q$ or $12q$, meson degrees of freedom in nuclei, the role of relativistic effects, etc.

(ii) The study of light nuclei provides an opportunity to elaborate the methods for the description of composite systems. Hadron physics is a physics of composite particles, quarks and gluons being constituents. Elaboration of new approaches for the description of composite systems based on the study of light nuclei has an undoubtful advantage that constituents (nucleons) are observed particles, with known interaction amplitudes.

This paper is devoted to simultaneous investigation of the two two-nucleon processes, namely, $NN \to NN$ at $0 \le T \le 1000$ MeV and $\gamma d \to pn$ at $0 \le E_\gamma \le 400$ MeV. This simultaneous investigation is not incidental: the $NN \to NN$ amplitude is a basic one for the study of the two-nucleon reactions. At the same time, the reaction $\gamma d \to pn$ is one of the simplest processes with two nucleons; therefore, the simultaneous analysis should clarify the points:

(i) To what extent and at what energies the nucleon-nucleon interaction governs the other processes induced by this interaction; and

(ii) What characteristics of the nucleon-nucleon interaction play the leading role.

For the deuteron photodisintegration at the photon energies in the laboratory frame $0 \le E_\gamma \le 400$ MeV, numerous experimental data exist, see [1]– [13] and references therein. This region covers both small energies, where quantum mechanics works, and comparatively large energies, where the relativistic effects and inelastic processes are important.

The reaction $\gamma d \to pn$ is investigated using dispersive integration technique, which is appropriate for the analysis of partial wave amplitudes:

(i) This technique is relativistic invariant;

(ii) It keeps under control all intermediate states allowing to take properly into account final state rescatterings which are determined by the right-hand singularities of the amplitudes [14];

(iii) In this technique there is no ambiguity related to the mass-off-shell amplitudes.

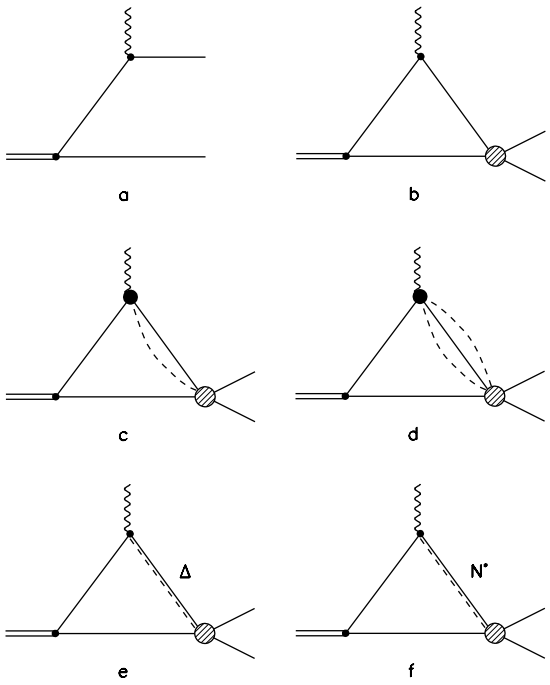

Fig. 1. Diagrams responsible for the deuteron photodisintegration process

The dispersion relation technique has much common with both non-relativistic quantum mechanics approach and light-cone variable technique, the methods which are widely used by non-perturbative QCD (or Strong-QCD[1]). A similarity of the dispersion relation and light-cone variable techniques was specially outlined in [16] where the Perturbative-QCD onset in meson form factors has been analysed.

Consider in more detail the mechanism of the deuteron photodisintegration, $\gamma d \to pn$, at $E_\gamma \leq 400$ MeV. The following processes contribute to this reaction: Fig. 1a — the deuteron break-up without nucleon interactions in the final state, Fig. 1b — the deuteron break-up followed by the rescattering of outgoing nucleons, Fig. 1c,d — the photoproduction of one or several mesons in the intermediate state, or — Fig. 1e,f — the photoexcitation of resonances, like Δ and $N^*(1400)$, followed by the transition of the produced particles into the pn state.

We start with the discussion of the nucleon–nucleon interaction. There is a striking property relevant to the hadron interaction at low and intermediate energies: in a wide energy range the nucleon interaction is almost elastic or quasi-elastic (this means an excitation of nucleons into highly located baryon states), i.e. with the energy growth the onset of genuine inelastic processes is delayed. Typical example is given by the deuteron channel (pn scattering in the ${}^3S_1$ and ${}^3D_1$ waves) where, though the threshold of the pion production is at $T = 290$ MeV, the phase shift analysis indicates that the inelasticity parameter is strongly suppressed up to $T = 1000$ MeV [17]. For other waves the inelasticities are related to baryon excitations;

[1] This terminology is suggested by F.E. Close [15]

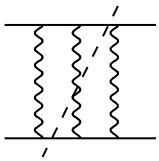

Fig. 2. Example of the Behte-Salpeter ladder diagram with nucleon rescatterings: the cutting of the diagram presents the connected inelastic processes

for instance, in the ${}^1D_2$ and ${}^3F_3$ waves the inelasticities are due to the transitions $NN \to N\Delta(1232)$. The same effect is seen in the pion-pion amplitude, where the inelasticity onset in the $I = 0$ S-wave starts at the energies much higher than the four-pion threshold. Presently there is quite a lot of evidences that this is a general feature of the processes at low and intermediate energies: inelasticities are mainly related to the transition of interacting hadron into an excited state, while the prompt production of new quark-antiquark pairs is suppressed. This property being observed several decades ago (see, for example, [18] and references therein) discussed starting from the early 60's; it is the foundation of the duality ideas and the models, such as that of Veneziano [19].

The direct way to perform a relativistic description of nucleon-nucleon interactions is to use the invariant Feynman technique that leads to the Bethe – Salpeter equation. However, the direct application of the Bethe – Salpeter equation to the nucleon–nucleon interaction faces problems related to the mass-off-shell amplitudes and meson production processes. Mass-off-shell phenomena are usually taken into account by the introduction of form factors, that undoubtedly affords an ambiguity in the quantitative representation of the process.

Another problem arises in the description of meson production within the Bethe-Salpeter equation. Indeed, the solution of this equation is represented as a sum of ladder diagrams of the type shown in Fig. 2. The cutting of ladder diagrams defines inelasticities of the amplitude; an example of such a cutting is shown in Fig. 2 by dashed line, it corresponds to the transition $NN \to NN + meson$. The problem is that forces in the deuteron channel related to the pion exchange are rather significant. Therefore, due to the cuttings of Fig. 2 – type, the Bethe — Salpeter equation leads to significant inelasticities which are switched on at invariant energies $\sqrt{s} = 2m + m_\pi, 2m + 2m_\pi$, etc. To suppress the early inelasticities, in line with the suppression of genuine inelastic processes, and at the same time to hold the non-small interaction related to pion-exchange forces, one should take into account other more complicated diagrams, in order 1) to cancel the right-hand s-channel singularities with the help of a destructive interference, and 2) to keep the neighbouring t-channel singularities (or left-hand ones) which respond to the non-small meson–exchange forces.

Moreover, an exact summation of ladder diagrams can hardly be performed in the realistic case, thus inducing necessary simplifications. One of them consists in the consideration of a potential-type interaction. Another one is an actual replacement of the constituent (nucleon) prop-

agator by its residue $(k^2 - m^2)^{-1} \to 2\pi i\theta(k_0)\delta(k^2 - m^2)$ [20]. However, this latter procedure leads to the anti-casual singularities of the amplitude; hence, one should take care these singularities be far from the region this approach pretends to describe.

A correct handling of the s- and t-channel singularities of the amplitude may be performed comparatively easily, in the framework of the dispersive N/D method [14], where the contributions of the left-hand singularities due to the t- and u-channel exchanges are independent of the right-hand ones which are related to the s-channel elastic and inelastic processes. An advantage of this technique is its relativistic invariance, together with the absence of a problem of the off-shell amplitude definition. For all intermediate particles the equality $k^2 = m^2$ is fulfilled, thus allowing us to describe interactions using mass-on-shell amplitudes. Moreover, in the dispersion relation technique there are no principal problems of the description of inelasticities related both to excited baryons and prompt meson production, because all the s-channel intermediate states are under control. This means that, when using dispersive integrals, one takes into account a certain set of the nearest singularities in due course.

It is also important that the dispersion relation technique allows us to determine the relativistic wave function (or vertex function) of the composite (deuteron-like) system. The description of the two-particle composite system within the dispersive N/D method was developed in [21], where the Lorentz-covariant amplitude for the two-particle composite system interacting with an external vector field has been written, and the ambiguities related to the dispersion relation subtractions have been eliminated on the basis of the gauge invariance and analyticity requirements. Therefore, while in the Feynman diagrammatic technique the gauge invariance is automatically fulfilled and the interaction amplitude obeys the Ward identity, in the dispersion relation technique these general properties of the theory should be considered as supplementary constraints. This is necessary payment for treating independently left- and right-hand singularities.

In [21] the dispersion relation analysis of the pn scattering amplitude in the ${}^3S_1 - {}^3D_1$ channels has been performed. Basing on the phase shift data, the pn scattering vertices have been constructed together with the deuteron vertex functions which are relativistic analogues of the deuteron wave functions. The use of deuteron wave function obtained in such a way allows us to describe well the deuteron form factors up to $Q^2 = 2$ GeV^2/c^2 as well as the deuteron binding energy and magnetic and quadrupole moments. A successful description of deuteron properties has been obtained taking properly into account the relativistic effects in the pn-component, without including non-nucleonic degrees of freedom into deuteron wave function.

Application of the dispersion relation technique to the description of the deuteron has a long history (see [22]): at the early stage, the deuteron form factor has been considered using the t-channel dispersion relation, thus bringing the t-channel anomalous singularity into consideration. The recent deuteron form factor description in terms of dispersive integrals [21] is based on the double dispersion representation in the deuteron channels, and it does not require special treatment of anomalous singularities. In this point the technique of [21] is analogous to the non-relativistic wave function technique. The detailed consideration of the composite–particle wave functions in the dispersive technique and its relation to the technique of light-cone variables may be found in [21], [23].

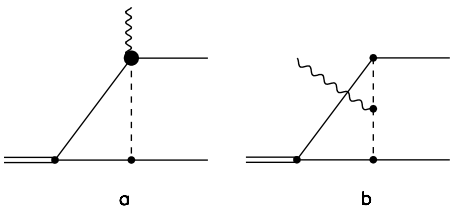

Fig. 3. Deuteron photodisintegration diagrams with meson exchange currents

Successful description of the elastic deuteron form factors within the dispersion relation technique gives rise to the problem of the application of this technique to other two-nucleon processes, in particular to the deuteron photodisintegration.

The reaction $\gamma d \to pn$ was studied during several decades [24]– [37] in the framework of other techniques, mainly in the quantum mechanical and Feynman diagram approaches. These investigations clarify many features of the reaction, among which — an important role of the meson exchange currents [31] (typical diagrams are shown in Fig. 3).

The analysis of the deuteron photodisintegration in the framework of the dispersion relation technique have been carried out in [38] starting from small energies, where the contribution of inelastic processes is negligible, with the subsequent energy increase. In the present paper we expand the analysis onto the region of the photon energy $E_\gamma \simeq 250 - 400$ MeV, where the production of the lightest baryons, $\Delta(1232)$ and $N^*(1400)$, is important.

The investigation of the reaction $\gamma d \to pn$ in the dispersive integral technique complements the investigations carried out within other approaches. This is related to the fact that similar processes from the point of view of their diagrammatic presentation may be treated in different approaches in their own ways. Such an example is meson–exchange currents, for in the dispersive technique they come from the contribution of anomalous t- and u-singularities to the amplitude $\gamma d \to pn$.

The paper is organized as follows.

In Chapt. 2 the nucleon-nucleon amplitude is analysed in the framework of the dispersion relation technique in the energy range up to $T = 1$ GeV. The aim of this analysis is to restore the nucleon-nucleon vertex functions, which play the role of forces of the quantum mechanics approach. These vertices are used in the next Chapter for the calculation of the final state interaction of nucleons in the deuteron photodisintegration. In Sect. 2.1 the operator expansion of nucleon-nucleon amplitude in partial

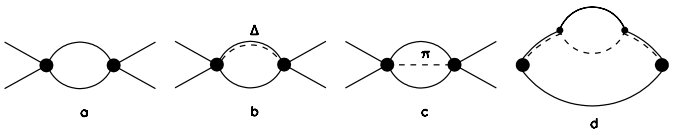

Fig. 4. Loop diagrams which correspond to the elastic rescattering **a**, intermediate-state production of the Δ isobar **b**, prompt pion production **c**, loop diagram used in the calculation of the two-particle phase space, with the account of the isobar width **d**

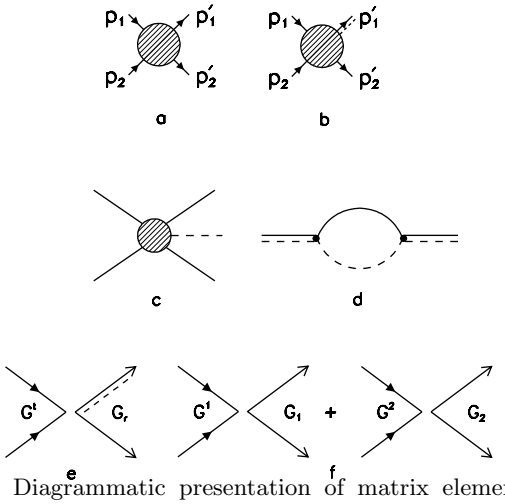

Fig. 5. Diagrammatic presentation of matrix elements for $NN \to NN$ **a**, $NN \to N\Delta$ **b**, $NN \to NN\pi$ **c**; loop diagram entering the vertex of the quasi-resonance decay $R \to \pi N$ **d**, presentation of vertices for nucleon–nucleon and nucleon–Δ interaction **e,f**

waves is done, together with the method of constructing covariant partial wave operators. In Sects. 2.2 and 2.3 the dispersion relation N/D method is described: it allows one to separate left- and right-hand singularities or, in other words, to single out the interaction forces from the production processes. Here the equation for the partial amplitude is written for one-channel case when inelastic processes are small, and it is also shown how to present the amplitude using the diagrammatic language. In Sect. 2.4, on the basis of phase shift analysis, the N/D amplitude is restored in the channels ${}^1P_1$ and ${}^3D_2$, where the inelasticity is small. In Sect. 2.5, the diagrammatic technique is generalized for the two-channel case. This allows us to include the inelasticity into nucleon-nucleon amplitude and to expand our analysis on other waves. The channels ${}^1D_2$, ${}^3P_2$ and ${}^3F_3$, with inelasticity related to the production of $\Delta(1232)$, are considered here. Based on the phase shift data for the channels NN and $N\Delta$, the amplitudes are restored for the coupled channels ${}^1D_2(NN) - {}^5S_2(N\Delta)$, ${}^3P_2(NN) - {}^5P_2(N\Delta)$ and ${}^3F_3(NN) - {}^5P_3(N\Delta)$. In Sect. 2.6 we briefly discuss the waves ${}^3S_1$ and ${}^3D_1$: these waves were investigated in detail in [21]. In Sect. 2.7 the structure of inelasticities in non-resonance channels ${}^1S_0$, ${}^3P_0$ and ${}^3P_1$ is studied: several mechanisms are considered, such as the production of $\Delta(1232)$, $N^*(1440)$ or the S-wave πN pair. The technique for the calculation of three-particle loop diagrams which are necessary for the description of inelastic processes is discussed in Appendix A, the N-function parameters are also given there.

In Chapt. 3 the amplitude $\gamma d \to pn$ is calculated, within the dispersion relation technique, up to the incident photon energy $E_\gamma = 400$ MeV. The photodisintegration amplitude is taken as a sum of diagrams shown in Fig. 1. Dashed blocks in Fig. 1b-f correspond to the nucleon final state interaction, which includes elastic–scattering diagrams of Fig. 4a–type and intermediate–state particle production processes of Fig. 4b,c–type. In Sect. 3.1 the pole diagram of Fig. 1a is written in terms of dispersion relation expression in the deuteron channel. In Sect. 3.2 the final state interaction is calculated for the channels ${}^1S_0$, ${}^3S_1 - {}^3D_1$, ${}^1P_1$, ${}^3P_0$, ${}^3P_1$, ${}^3P_2$, ${}^3D_2$, ${}^1D_2$ and ${}^3F_3$ taking the account of diagrams of Fig. 4a-type only (i.e. neglecting inelastic rescatterings). Such an approximation allows one to describe the photodisintegration amplitude up to $E_\gamma = 10$ MeV. In Sect. 3.3 the inelasticities related to the production of $\Delta(1232)$ are included into the final–state channels ${}^3P_2$, ${}^1D_2$ and ${}^3F_3$. Two mechanisms contribute to the intermediate Δ-production: the Δ-production in the final state nucleon-nucleon interaction block (Fig. 4b) and the prompt Δ-production by photon (Fig. 1e). In Sect. 3.4 the contribution of inelasticities into $\gamma d \to pn$ is calculated for nucleon–nucleon waves ${}^1S_0$, ${}^3P_0$ and ${}^3P_1$. It is shown that the process $\gamma d \to pn \to X \to pn$, where X is one of the inelastic states $(N\pi)_S N$, $N^*(1400)N$ or $N\Delta$, dominates in these waves. These transitions are important at $E_\gamma = 50 - 100$ MeV, while the transition $\gamma d \to N\Delta \to pn$ in the waves ${}^1D_2$, ${}^3P_2$ and ${}^3F_3$, Fig. 1e, is important at $E_\gamma \simeq 300 - 400$ MeV.

The detailed discussion of the results is presented in Chap. 4.

2 Dispersion relation representation of nucleon-nucleon scattering amplitude

2.1 Nucleon–nucleon vertex operators for partial amplitudes

Consider the structure of multipole operators for the NN partial scattering amplitudes. There are two ways for the presentation of the amplitude expanded in multipoles. Standard matrix element for the transition $NN \to NN$ (see Fig. 5a) is as follows:

$$(\bar\Psi(p_1')Q^b\Psi(p_1))\,(\bar\Psi(p_2')\tilde Q^b\Psi(p_2))\,, \qquad (2.1)$$

where Q^b and $\tilde Q^b$ are multipole operators. However, in the dispersive technique it is more convenient to use charge–conjugated fields:

$$\Psi_c(-p_2') = -\bar\Psi(p_2')C\,, \qquad \bar\Psi_c(-p_2) = C\Psi(p_2)\,, \qquad (2.2)$$

where C is charge–conjugation operator. Using the Fierz transformation [39], $\Psi(p_1) \leftrightarrow \Psi_c(p_2')$, one gets

$$(\bar\Psi(p_1')\tilde Q^b\Psi_c(-p_2'))\,(\bar\Psi_c(-p_2)Q^b\Psi(p_1))\,, \qquad (2.3)$$

where Q^b, $\tilde{Q}^b$ is another set of operators corresponding to the $^{2S+1}L_J$ NN state. The whole amplitude, $A(s,t)$, depends on $s=(p_1+p_2)^2$ and $t=(p_1-p_1')^2$ and can be represented as a sum of partial amplitudes, $A^b(s)$, as follows:

$$A(s,t)=\sum_b(\bar{\Psi}(p_1')I^b_{ij}\tilde{Q}^b_{\mu\nu\ldots}\Psi_c(-p_2'))\times(\bar{\Psi}_c(-p_2)I^b_{ij}Q^b_{\mu\nu\ldots}\Psi(p_1))A^b(s)\,. \quad (2.4)$$

Here $Q^b_{\mu\nu\ldots}$ and $\tilde{Q}^b_{\mu\nu\ldots}$ are left and right operators of the partial amplitude, $\mu,\nu\ldots$ are indices related to the state $^{2S+1}L_J$, and I^b_{ij} is isotopic operator. Summation in (2.4) is carried out over the whole set of operators $Q^b_{\mu\nu\ldots}$.

Consider the structure of the $Q^b_{\mu\nu\ldots}$ operator. For the spin-$\frac{1}{2}$ particles, these operators are constructed using metrical tensor $g_{\mu\nu}$, antisymmetrical tensor $\varepsilon_{\mu\nu\alpha\beta}$, γ-matrices and momenta $k_\mu=\frac{1}{2}(p_1-p_2)_\mu$ and $P_\mu=(p_1+p_2)_\mu$. Let us introduce the tensor $T_{\mu'\nu'\ldots,\mu\nu\ldots}$ related to the two-nucleon loop diagram:

$$\langle Sp[-(\hat{p}_1+m)\tilde{Q}^b_{\mu\nu\ldots}(-\hat{p}_2+m)Q^a_{\mu'\nu'\ldots}]\rangle=\delta^{ab}T_{\mu'\nu'\ldots,\mu\nu\ldots}\rho(s). \quad (2.5)$$

Here δ^{ab} is the Kronecker tensor, the brackets $\langle\cdots\rangle$ denote the integration over the two–particle phase space, $d\Phi(p_1,p_2)$:

$$d\Phi(p_1,p_2)=\frac{1}{2}\,\frac{d^4p_1d^4p_2}{(2\pi)^6}(2\pi)^4\delta^4(P-p_1-p_2)\times\delta(m^2-p_1^2)\delta(m^2-p_2^2), \quad (2.6)$$

where

$$\int d\Phi(p_1,p_2)=\frac{1}{16\pi}\sqrt{\frac{s-4m^2}{s}}\equiv\rho(s)\,. \quad (2.7)$$

We impose the following normalization constraint:

$$T_{\alpha\beta\cdots,\mu\nu\ldots}T_{\mu'\nu'\ldots,\alpha\beta\ldots}=T_{\mu'\nu'\ldots,\mu\nu\ldots}\,. \quad (2.8)$$

For the states with total angular momenta $J=0,1,2$, the T-operators are equal to:

$$\begin{aligned}&J=0: && T=1,\\ &J=1: && T_{\mu',\mu}=g^\perp_{\mu'\mu},\\ &J=2: && T_{\mu'\nu',\mu\nu}=\tfrac{1}{2}\left(g^\perp_{\mu\mu'}g^\perp_{\nu\nu'}+g^\perp_{\mu\nu'}g^\perp_{\nu\mu'}-\tfrac{2}{3}g^\perp_{\mu\nu}g^\perp_{\mu'\nu'}\right),\end{aligned} \quad (2.9)$$

where $g^\perp_{\mu\nu}=g_{\mu\nu}-P_\mu P_\nu/s$.

With these requirements, we get the following set of the pn vertex operators for the state $^{2S+1}L_J$ with isotopic spin $I=0,1$:

$$\begin{aligned}
&^1S_0(I=1): Q=\tfrac{1}{\sqrt{2s}}\gamma_5,\ \tilde{Q}=-Q,\\
&^3P_0(I=1): Q=\frac{1}{\sqrt{2(s-4m^2)}},\ \tilde{Q}=Q,\\
&^3S_1(I=0): Q_\mu=\tfrac{1}{\sqrt{2s}}\Gamma_\mu,\ \tilde{Q}_\mu=-Q_\mu,\\
&^3D_1(I=0): Q_\mu=\tfrac{1}{2\sqrt{s}}\left[4k_\mu\tfrac{m+\sqrt{s}}{s-4m^2}+\gamma^\perp_\mu\right],\ \tilde{Q}_\mu=-Q_\mu,\\
&^1P_1(I=0): Q_\mu=\sqrt{\tfrac{3}{2s(s-4m^2)}}\gamma_5k^\perp_\mu,\ \tilde{Q}_\mu=Q_\mu,\\
&^3P_1(I=1): Q_\mu=\sqrt{\tfrac{3}{s^2(s-4m^2)}}\varepsilon_{\mu\alpha\beta\delta}\gamma_\alpha P_\beta k_\delta,\ \tilde{Q}_\mu=-Q_\mu,\\
&^3P_2(I=1): Q_{\mu\nu}=\sqrt{\tfrac{3}{2s(s-4m^2)}}\left[k^\perp_\mu\Gamma_\nu+k^\perp_\nu\Gamma_\mu-\tfrac{2}{3}(k^\perp\Gamma)g^\perp_{\mu\nu}\right],\ \tilde{Q}_{\mu\nu}=Q_{\mu\nu},\\
&^1D_2(I=1): Q_{\mu\nu}=\tfrac{\sqrt{60}}{\sqrt{s}(s-4m^2)}\gamma_5\left[k^\perp_\nu k^\perp_\mu-\tfrac{k^2}{3}g^\perp_{\mu\nu}\right],\ \tilde{Q}_{\mu\nu}=-Q_{\mu\nu},\\
&^3D_2(I=0): Q_{\mu\nu}=\tfrac{\sqrt{10}}{s(s-4m^2)}\left[k^\perp_\nu\varepsilon_{\mu\alpha\beta\delta}\gamma_\alpha P_\beta k_\delta+k^\perp_\mu\varepsilon_{\nu\alpha\beta\delta}\gamma_\alpha P_\beta k_\delta\right],\ \tilde{Q}_{\mu\nu}=Q_{\mu\nu},\\
&^3F_3(I=1): Q_{\mu\nu\chi}=\sqrt{\tfrac{3}{70s^2(s-4m^2)^3}}\\
&\quad\times\left[K^a_{\mu\nu}\varepsilon_{abc\chi}\gamma_bP_c+K^a_{\nu\chi}\varepsilon_{abc\mu}\gamma_bP_c+K^a_{\chi\mu}\varepsilon_{abc\nu}\gamma_bP_c\right],\\
&\quad\tilde{Q}_{\mu\nu\chi}=Q_{\mu\nu\chi}\,.
\end{aligned} \quad (2.10)$$

Here $k^\perp_\mu=k_\mu-(Pk)P_\mu/s$, $\gamma^\perp_\mu=\gamma_\mu-\hat{P}P_\mu/s$, $\Gamma_\mu=\gamma^\perp_\mu-2k^\perp_\mu/(2m+\sqrt{s})$ and $K_{\mu\nu\chi}=k_\mu k_\nu k_\chi-\frac{k^2}{5}(k_\mu g^\perp_{\nu\chi}+k_\nu g^\perp_{\chi\mu}+k_\chi g^\perp_{\mu\nu})$. Let us stress that in (2.10) we have introduced left and right operators because the trace in (2.5) may be the negative in the technique used: this leads to different left and right operators.

It should be noted that Ψ_c and Ψ have opposite parities, so $\bar{\Psi}_c\gamma_5\Psi$ is a scalar and $\bar{\Psi}_c\Psi$ is a pseudoscalar.

For the singlet and triplet isotopic states, the isotopic operators are:

$$I=0:\quad I_{ij}=\frac{\delta_{ij}}{\sqrt{2}},\qquad I=1:\quad \boldsymbol{I}_{ij}=\frac{\boldsymbol{\tau}_{ij}}{\sqrt{2}}, \quad (2.11)$$

where $\boldsymbol{\tau}_{ij}$ are Pauli matrices.

Consider as an example the construction of the operator $Q_{\mu\nu}$ for the $^3P_2$ state: the total momentum $J=2$, so this operator is traceless symmetrical tensor of the second rank constructed of $k^\perp_\mu$ (the P wave state) and Γ_ν (the spin–triplet state). Therefore, the operator for the $^3P_2$ state is proportional to $O_{\mu\nu}=k^\perp_\mu\Gamma_\nu+k^\perp_\nu\Gamma_\mu-\frac{2}{3}(k^\perp\Gamma)g^\perp_{\mu\nu}$, where $Q_{\mu\nu}=N(s)O_{\mu\nu}$ and $N(s)$ is normalization constant. We have:

$$\langle Sp[-(\hat{p}_1+m)\tilde{O}_{\mu\nu}(-\hat{p}_2+m)O_{\mu'\nu'}]\rangle=\frac{2}{3}s(s-4m^2)T_{\mu\nu,\mu'\nu'}\rho(s). \quad (2.12)$$

Therefore, the operator for the $^3P_2$ state is:

$$Q_{\mu\nu}=\sqrt{\frac{3}{2s(s-4m^2)}}O_{\mu\nu}. \quad (2.13)$$

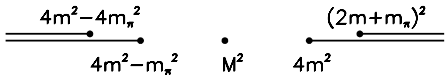

Fig. 6. Complex s-plane and the position of the partial amplitude singularities: (from right to left) right-hand side singularities at $s = 4m^2,\ (2m + m_\pi)^2$ ..., the position of pole, and left-hand ones at $s = 4m^2 - m_\pi^2,\ 4m^2 - 4m_\pi^2$ ...

Likewise, one can construct vertex operators for all partial amplitudes.

Partial amplitude $A^b(s)$ for the fixed state is obtained by projecting the whole amplitude $A(s,t)$ given by (2.4) on this state. Corresponding conjugate operator is as follows:

$$(\bar\Psi(p_1)Q^b_{\mu\nu\ldots}\Psi_c(-p_2))\,(\bar\Psi_c(-p_2')\tilde Q^b_{\mu'\nu'\ldots}\Psi(p_1')). \qquad (2.14)$$

Thus, we have:

$$4T_{\mu\nu\ldots\mu'\nu'\ldots}\rho(s)A^b(s)\rho(s) = \int d\Phi(p_1,p_2)d\Phi(p_1',p_2') \times (\bar\Psi(p_1)Q^b_{\mu\nu\ldots}\Psi_c(-p_2)) \times A(s,t)\,(\bar\Psi_c(-p_2')\tilde Q^b_{\mu'\nu'\ldots}\Psi(p_1')). \qquad (2.15)$$

After integrating over azimuthal angle, the following expression for $A^b(s)$ is obtained:

$$4T_{\mu\nu\ldots\mu'\nu'\ldots}A^b(s) = \int_{-1}^{1}\frac{dz}{2}(\bar\Psi(p_1)Q^b_{\mu\nu\ldots}\Psi_c(-p_2)) \times, A(s,t)(\bar\Psi_c(-p_2')\tilde Q^b_{\mu'\nu'\ldots}\Psi(p_1')), \qquad (2.16)$$

where z is the cosine of the angle between $\boldsymbol{p}_1$ and $\boldsymbol{p}_1'$ in the center-of-mass system of particles 1 and 2: $z = 1 + 2t/(s - 4m^2)$.

2.2 Left- and right-hand singularities and the unitarity of partial amplitudes

In this Section we remind the analytic structure of the amplitude when nucleons interact by the pion exchange (m_π is pion mass). In this case the amplitude has a pole in the t-channel at $t = m_\pi^2$, as well as threshold singularities at $t = (nm_\pi)^2$ ($n = 2, 3, ...$). In the s-channel the amplitude has a singularity at $s = 4m^2$ related to nucleon rescattering and branching points $s = (2m + nm_\pi)^2$ related to inelastic channels. For the deuteron channel a bound state with mass M exists: the amplitude has a pole singuliarity at $s = M^2$. The s-channel partial amplitudes have the same s-channel singuliarities (right-hand ones) as the whole amplitude, $A(s,t)$. Besides, partial amplitudes have left-hand singularities which correspond to the t- and u-channel singuliarities of $A(s,t)$ with branching points $s = 4m^2 - m_\pi^2 n^2$ — see Fig. 6. The neglecting of inelasticities means that we neglect all the right-hand cuts, except for the first one, with the branching point at $s = 4m^2$.

Consider the unitarity of the partial amplitude in the physical region (the upper edge of the elastic cut). One has $SS^+ = 1$ with

$$S = \mathbf{1} + i(2\pi)^4\delta^4(p_1 + p_2 - p_1' - p_2')A(s,t). \qquad (2.17)$$

Using the decomposition of the amplitude (2.4) and the equation (2.5), we get the unitarity relation for the partial amplitude:

$$Im\,A^b(s) = \rho(s)|A^b(s)|^2. \qquad (2.18)$$

2.3 One–channel scattering in the diagrammatic dispersion relation technique

According to N/D method [14], the partial amplitude $A(s)$ can be represented as a ratio of two functions (here and below the index b of the partial NN state is omitted):

$$A(s) = \frac{N(s)}{D(s)}, \qquad (2.19)$$

with $N(s)$ containing left-hand sinquliarities and $D(s)$ containing right-hand ones only. It follows from the unitarity condition (2.18) that

$$Im\,D(s) = -\rho(s)N(s). \qquad (2.20)$$

The normalization used for $D(s)$ reads: $D(s) \to 1$ at $s \to \infty$. It is also assumed that there are no CDD-poles [40] in the amplitude. In this way one gets:

$$D(s) = 1 - \int_{4m^2}^{\infty}\frac{ds'}{\pi}\frac{\rho(s')N(s')}{s' - s} = 1 - B(s). \qquad (2.21)$$

One can restore the N-function using experimental data, thus solving the problem of finding an amplitude with correct analytic properties in the vicinity of the point $s = 4m^2$. However, to describe the nucleon-nucleon system (say, deuteron) which interacts with an external field, it is convenient to introduce vertices, which, in the case of a deuteron, play the role of wave functions [41]. In the simplest case, the vertex function may be defined as follows:

$$G(s) = \sqrt{N(s)}\,. \qquad (2.22)$$

Then $A(s)$ can be written as a sum of dispersive diagrams shown in Fig. 7a.

$$A(s) = G(s)(1 + B(s) + B(s)^2 + \cdots)G(s), \qquad (2.23)$$

where $B(s)$ corresponds to the one–loop diagram with the vertex $G(s)$.

Consider the one–loop dispersive diagram and its connection with the Feynman one–loop diagram. The Feynman integral reads:

$$A_F = \int\frac{d^4k}{(2\pi)^4 i} \qquad (2.24)$$
$$\frac{a(k_1^2,(P-k_1)^2;k^2,(P-k)^2)a(k^2,(P-k)^2;k_2^2,(P-k_2)^2)}{(m^2-k^2)(m^2-(P-k)^2)}.$$

Here $a(k_1^2,(P-k_1)^2;k^2,(P-k)^2)$ is an irreducible block, without two-particle intermediate states. The receipt for the transition from Feynman integral to the dispersive one is the following. We need:

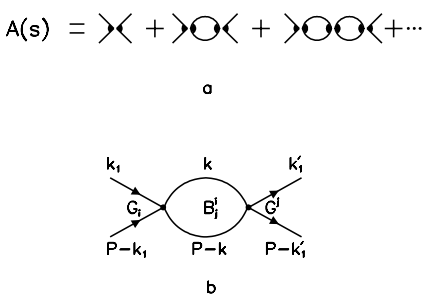

Fig. 7. Dispersion relation loop diagrams: **a** representation of the partial amplitude as a set of loop diagrams, **b** one–loop diagram with right (G_i) and left (G^j) vertices: $G_j B_j^i G^i$

1) To neglect the right-hand multiparticle singularities in the block a;

2) To factorize the block a:

$$a(k_1^2,(P-k_1)^2;k^2,(P-k)^2) \to G(k_1^2,(P-k_1)^2)G(k^2,(P-k)^2); \quad (2.25)$$

3) To calculate the imaginary part of the one-loop Feynman diagram, considering the intermediate state with the energy $\sqrt{s}$ as real one ($s>4m^2$):

$$\frac{d^4k}{(2\pi)^4 i}\frac{1}{(m^2-k^2)(m^2-(P-k)^2)} \to \frac{d^4k}{(2\pi)^4 i}\frac{1}{2i}(2\pi i)^2\theta(k_0)\delta(m^2-k^2) \theta(P_0-k_0)\delta(m^2-(P-k)^2)=\rho(s); \quad (2.26)$$

4) To restore the B-function using dispersion relation integral over the imaginary part related to the elastic cut, $disc\, A_F$:

$$\int_{4m^2}^{\infty}\frac{ds'}{\pi}\frac{\rho(s')}{s'-s}disc\, A_F(s') = \int_{4m^2}^{\infty}\frac{ds'}{\pi}\frac{G^2(s')\rho(s')}{s'-s}. \quad (2.27)$$

Finally, we get $G(s)B(s)G(s)$.

The above consideration demonstrates the applicability limit for (2.24): the basic assumption is a factorization of the block a.

General method of making factorization for the t- and u-channel meson exchange interactions has been developed in [41]. Generally, for the description of composite systems one should introduce several vertex functions G_i related to the separable interaction V_i: $N_i \to V_i = G_i G^i$, where the left vertex function, G_i, and the right one, G^i, may be different. It is convenient to introduce the amplitudes a_i which do not contain the right vertices G^i. The whole amplitude and auxiliary amplitudes a_i are related as:

$$A = \sum_i a_i G^i. \quad (2.28)$$

The amplitudes a_i obey a set of linear equations:

$$a_i = \sum_j a_j B_i^j + G_j\delta_{ij}\,, \quad (2.29)$$

where (see Fig. 7b)

$$B_i^j(s) = \int_{4m^2}^{\infty}\frac{ds'}{\pi}\frac{G^j(s')\rho(s')G_i(s')}{s'-s}\,. \quad (2.30)$$

Rewriting (2.29) in a matrix form, one has

$$\hat{a} = \hat{B}\hat{a} + \hat{g}\,, \quad (2.31)$$

where

$$\hat{a} = \begin{bmatrix} a_1 \\ a_2 \\ . \end{bmatrix}, \quad \hat{g} = \begin{bmatrix} G^1 \\ G^2 \\ . \end{bmatrix}, \quad \hat{B} = \begin{bmatrix} B_1^1 & B_1^2 & . \\ B_2^1 & B_2^2 & . \\ . & . & . \end{bmatrix}. \quad (2.32)$$

Final expression for the partial amplitude reads:

$$A = \hat{g}^T(I-B)^{-1}\hat{g}\,, \quad (2.33)$$

where

$$\hat{g}^T = [G_1, G_2, \cdots]\,. \quad (2.34)$$

The amplitude obtained in such a way is unitary; it may be derived directly from the unitarity condition.

Now let us explain how the scattering amplitude discussed above may be written in terms of the energy-off-shell Bethe-Salpeter equation. We need to introduce the energy-off-shell scattering amplitude:

$$A(s,s_1) = \sum_i a_i(s)G^i(s_1). \quad (2.35)$$

Using (2.31), one can write this amplitude as

$$A(s,s_1) = \int_{4m^2}^{\infty}\frac{ds'}{\pi}\frac{\rho(s')}{s'-s}A(s,s')V(s',s_1) + V(s,s_1). \quad (2.36)$$

This is the dispersive Bethe-Salpeter equation for $A(s,s_1)$, where the effective interaction is

$$V(s,s_1) = \sum_i G_i(s)G^i(s_1). \quad (2.37)$$

The suggested diagrammatic technique is a modification of the standard N/D method: this technique is suitable for the description of interaction with the external field.

2.4 One–channel approach for the waves $^1P_1$ and $^3D_2$

In the waves $^1P_1$ and $^3D_2$ the inelasticity is small, and corresponding amplitudes can be described in the one–channel approximation. We restore vertex functions for the pn scattering relying upon the phase shift analysis data [17]. The G-function is determined by the left-hand singularities, therefore it is given as a dispersive integral along the left-hand cuts:

$$G(s) = \int_{-\infty}^{s_L}\frac{ds'}{\pi}\frac{disc\, G(s')}{s-s'}, \quad (2.38)$$

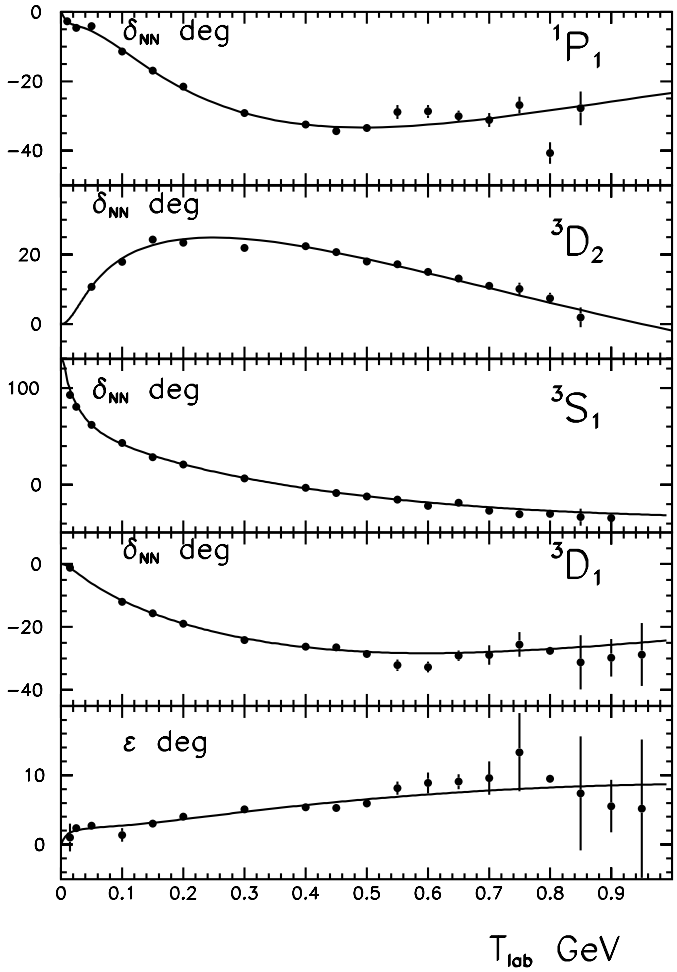

Fig. 8. Results of the fit for the phase shifts, δ_{NN}, for nucleon-nucleon scattering. $T_{\rm lab}$ is the kinetic energy of incident proton in the laboratory system: the waves ${}^1P_1$, ${}^3D_2$ and coupled channels ${}^3S_1 - {}^3D_1$ (phase shifts δ_{NN} and mixing parameter ε)

where $s_L = 4m^2 - m_\pi^2$ is the location of the nearest pion branching point. Below, to simplify a cumbersome calculations, we replace the integartion in (2.38) by the summation:

$$G_i(s) = \sum_{j=1}^{6} \frac{\gamma_j^i}{s - s_j^i}\,, \qquad s_j^i = s_0^i - h^i(j-1), \qquad (2.39)$$

with the poles s_j^i placed on the left from s_L.

The values of parameters γ_j^i, h^i and s_0^i obtained by fitting the phase shift data are discoursed in Appendix A. The results of the phase shift fit together with the experimental data are shown in Fig. 8.

2.5 Two–channel scattering, NN and $N\Delta$: the waves ${}^1D_2$, ${}^3P_2$ and ${}^3F_3$

In this Section we consider the inelasticity in the nucleon-nucleon amplitude due to the production of the isobar $\Delta(1232)$. Here nucleon-nucleon amplitude is treated as a two-channel one (the channels NN and $N\Delta$). We analyse the coupled channels: ${}^1D_2(NN) - {}^5S_2(N\Delta)$, ${}^3P_2(NN) - {}^5P_2(N\Delta)$ and ${}^3F_3(NN) - {}^5P_3(N\Delta)$.

The matrix element for the $NN \to N\Delta$ transition (see Fig. 5b for the momentum notation) is written in the form

$$(\bar\Psi^\mu(p_1')\tilde Q^a_{\alpha\beta,\mu} T_0 \Psi_c(-p_2'))(\bar\Psi_c(-p_2) Q^b_{\alpha\beta} I \Psi(p_1)) A^{ab}(s). \qquad (2.40)$$

Here $\tilde Q^a$ and Q^b are vertex operators for the states a and b. T_λ and I are isotopic operators in the $N\Delta$ and NN channels, correspondingly. $A_{ab}(s)$ is partial amplitude for the transition *state* $b \to$ *state* a. Ψ_μ is the wave function for the spin-$\frac{3}{2}$ particle; Ψ_μ obeys the equations:

$$p_\mu \Psi_\mu(p) = 0, \qquad \gamma_\mu \Psi_\mu(p) = 0. \qquad (2.41)$$

For the $N\Delta$ states, vertex operators are as follows:

$$\begin{aligned}
{}^5S_2(N\Delta):\ \tilde Q_{\alpha\beta,\mu} &= \frac{1}{\sqrt{\Omega_1}}\left[\tilde\Gamma_\alpha g^\perp_{\beta\mu} + \tilde\Gamma_\beta g^\perp_{\alpha\mu} - \frac{2}{3} g^\perp_{\alpha\beta}\tilde\Gamma_\mu\right] \\
&\equiv S_{\alpha\beta,\mu}, \\
{}^5P_2(N\Delta):\ \tilde Q_{\alpha\beta,\mu} &= \frac{1}{\sqrt{\Omega_2}}\left[\varepsilon_{abc\alpha} k_a^t P_b S_{c\beta,\mu}\right. \\
&\quad \left. +\ \varepsilon_{abc\beta} k_a^t P_b S_{c\alpha,\mu}\right], \qquad (2.42) \\
{}^5P_3(N\Delta):\ \tilde Q_{\alpha\beta\gamma,\mu} &= \frac{1}{\sqrt{\Omega_3}}\left[S_{\alpha\beta,\mu} k_\gamma^t + S_{\beta\gamma,\mu} k_\alpha^t + S_{\gamma\alpha,\mu} k_\beta^t\right. \\
&\quad \left. -\ \frac{2}{5} k_\nu^t (S_{\alpha\nu,\mu} g^\perp_{\beta\gamma} + S_{\beta\nu,\mu} g^\perp_{\gamma\alpha} + S_{\gamma\nu,\mu} g^\perp_{\alpha\beta})\right].
\end{aligned}$$

Here Ω_i is a normalizing factor; the momenta are defined as $P = p_1 + p_2$, $k = \frac{1}{2}(p_1 - p_2)$, $s = P^2$, $k^t = \frac{1}{2}(p_1 - p_2) - \frac{1}{2s}(m_\Delta^2 - m^2)P$, where m_Δ is the Δ-isobar mass; $k_\mu^\perp$, $\gamma_\mu^\perp$ and $g^\perp_{\alpha\beta}$ are introduced in Sect. 2.1, while $\tilde\Gamma_\mu$ is defined as

$$\tilde\Gamma_\mu = \gamma_\mu^\perp - \frac{2k_\mu^\perp}{m + m_\Delta + \sqrt{s}}\,. \qquad (2.43)$$

The NN vertex operators, Q^b, for ${}^1D_2$, ${}^3P_2$ and ${}^3F_3$ states are given by equation (2.10).

The isotopic operator T_0 for the states $\Delta^+ n$ and $\Delta^0 p$ is defined as

$$T_0^+ = \frac{1}{\sqrt{2}}\begin{bmatrix} 0 & 0 \\ 1 & 0 \\ 0 & 1 \\ 0 & 0 \end{bmatrix}, \quad T_0 = \frac{1}{\sqrt{2}}\begin{bmatrix} 0 & 1 & 0 & 0 \\ 0 & 0 & 1 & 0 \end{bmatrix}. \qquad (2.44)$$

Partial amplitude A is 2×2 matrix. It is related to the 2×2 S-matrix as follows:

$$S = I + 2i\sqrt{\rho} A \sqrt{\rho}\,, \qquad (2.45)$$

where $\sqrt{\rho}$ is the matrix of square roots of phase space factors:

$$\sqrt{\rho} = \begin{bmatrix} \sqrt{\rho_{NN}} & 0 \\ 0 & \sqrt{\rho_{N\Delta}} \end{bmatrix}. \qquad (2.46)$$

As before (see Sect. 2.3), the partial amplitude is represented in the form:

$$A = \hat{g}^T (I - \hat{B})^{-1} \hat{g}\,, \tag{2.47}$$

but with another structure of vertex operators:

$$\hat{g} = \begin{bmatrix} G^N & 0 \\ G^t & 0 \\ 0 & G^r \\ 0 & G^\Delta \end{bmatrix}, \qquad \hat{g}^T = \begin{bmatrix} G_N & 0 & G_t & 0 \\ 0 & G_r & 0 & G_\Delta \end{bmatrix}, \tag{2.48}$$

and B-matrix

$$\hat{B} = \begin{bmatrix} B_{NNN} & 0 & B_{NNt} & 0 \\ B_{tNN} & 0 & B_{tNt} & 0 \\ 0 & B_{r\Delta r} & 0 & B_{r\Delta\Delta} \\ 0 & B_{\Delta\Delta r} & 0 & B_{\Delta\Delta\Delta} \end{bmatrix},$$

$$B_{ijk}(s) = \int_{T_j}^{\infty} \frac{ds'}{\pi} \frac{G^i(s')\rho_j(s')G_k(s')}{s - s'}\,. \tag{2.49}$$

Here $G_N G^N$, $G_\Delta G^\Delta$, $G_r G^t$ and $G_t G^r$ are the N-functions for the transitions $NN \to NN$, $N\Delta \to N\Delta$, $NN \to N\Delta$ and $N\Delta \to NN$, correspondingly (see Fig. 5e), $T_1 = 4m^2$, $T_2 = (2m + m_\pi)^2$. In our fit we put $G^r = G_r$ and $G^t = G_t$; as it was in previous Section, the two-vertex form is used for the transition $NN \to NN$: $G_N G^N = G_1 G^1 - G_2 G^2$ — Fig. 5f.

For vertex functions the parametrization (2.39) is used. Parameters for G are found using nucleon-nucleon and nucleon-isobar phase shifts, δ_{NN} and $\delta_{N\Delta}$, and the inelasticity parameter η which are defined as

$$S_{11} = \eta e^{2i\delta_{NN}}, \quad |S_{12}| = |S_{21}| = \sqrt{1 - \eta^2},$$
$$S_{22} = \eta e^{2i\delta_{N\Delta}}.$$

Here indices 1 and 2 refer to the channels NN and $N\Delta$. The description of the phase shift data in the coupled channels ${}^1D_2 - {}^5S_2$, ${}^3P_2 - {}^5P_2$ and ${}^3F_3 - {}^5P_3$ is shown in Fig. 9 together with the experimental data [42].

2.6 Coupled channels ${}^3S_1$ and ${}^3D_1$

In Fig. 8 the coupled channels ${}^3S_1 - {}^3D_1$ are drawn, for which the inelasticity is small, though the connection of channels is important, so the two-channel approach must be applied here [21].

2.7 Models for the inelasticity in the ${}^1S_0$ wave

According to [17], the mechanism of inelasticity in the waves ${}^1S_0$, ${}^3P_0$ and ${}^3P_1$ differs from the inelasticity in the channels ${}^1D_2$, ${}^3P_2$ and ${}^3F_3$, and the amplitude has a non-resonance behaviour.

Here we consider several models for inelasticity in the ${}^1S_0$ wave. First, we suggest that the inelasticity comes due to the production of $\Delta(1232)$. Second, we consider the production of $N^*_{11}(1440)$ as a source of inelasticity. This resonance is heavier than $\Delta(1232)$, but it has larger width and the transition amplitude ${}^1S_0(NN) - {}^1S_0(NN^*)$ is not suppressed near the threshold. Third, the prompt pion production in the πN S-wave is assumed. It should be noted that both the 1st and 2nd variants correspond to the production of the πN-state in the P-wave.

1) $\Delta(1232)$**-isobar production**

Matrix element for the transition ${}^1S_0(NN) - {}^5D_0(N\Delta)$ is determined by (2.40). The vertex operator for the ${}^5D_0$ wave is

$${}^5D_0(N\Delta): \quad Q_\mu = \frac{1}{\sqrt{\Omega}} \left[\tilde{\Gamma}_\alpha g^\perp_{\beta\mu} + \tilde{\Gamma}_\beta g^\perp_{\alpha\mu} - \frac{2}{3} g^\perp_{\alpha\beta} \tilde{\Gamma}_\mu \right] \times K_{\alpha\beta}, \tilde{Q}_\mu = -Q_\mu, \tag{2.50}$$

where Ω is the normalization factor and

$$K_{\alpha\beta} = k^t_\alpha k^t_\beta - \frac{1}{3} k^{t2} g^\perp_{\alpha\beta}\,. \tag{2.51}$$

2) **Production of** $N^*(1440)$

Matrix element for the transition $NN \to NN^*$ is written in the form similar to (2.40):

$$(\bar{\Psi}_{N^*}(p'_1)\tilde{Q}^a I^i \Psi_c(-p'_2))(\bar{\Psi}_c(-p_2) Q^b I^i \Psi(p_1)) A^{ab}(s)\,. \tag{2.52}$$

The resonance $N^*(1440)$ has the same quantum numbers as a nucleon, so vertex operator for the NN^* state is:

$${}^1S_0(NN^*): \quad Q = \frac{1}{\sqrt{\Omega}} \gamma_5, \quad \tilde{Q} = -Q. \tag{2.53}$$

3) **Production of the** $(\pi N)_S$**-pair in the** $J^P = \frac{1}{2}^-$ **state**

Since the lightest resonances in the πN system, with quantum numbers $J^P = \frac{1}{2}^-$, are located far from the pion-nucleon threshold, we deal here with the case of the prompt non-resonance pion production (Fig. 5c). Nevertheless, we approximate the πN pair by a remote quasi-resonance R, with an energy–dependent width. This enables us to operate with the two-particle intermediate states using the same technique as is used for $\Delta(1232)$ and $N^*(1440)$.

Consider the vertex of the quasi-resonance decay $R \to \pi N$: $\Gamma_\pi = c_\pi \boldsymbol{\tau}$. The width of the quasi-resonance R, Γ^w_R, is defined by its decay into pion and nucleon. This allows us to relate the quantities c_π and Γ^w_R. The resonance propagator is written as:

$$\frac{(\hat{p} + M_R)}{M_R^2 - p^2 - B(p^2)}\,, \tag{2.54}$$

where $B(p^2)$ corresponds to the pion–nucleon loop diagram (Fig. 5d). Real part of the loop diagram redetermines the mass of the quasi–resonance M_R, and imaginary part of $B(p^2)$ provides its width. Let us rewrite the propagator (2.54) as a series:

$$\frac{(\hat{p} + M_R)}{M_R^2 - p^2 - iM_R\Gamma_R} = \frac{(\hat{p} + M_R)}{(M_R^2 - p^2)} + \frac{(\hat{p} + M_R)}{(M_R^2 - p^2)} \times i\Gamma^w_R M_R \frac{1}{(M_R^2 - p^2)} + ... \tag{2.55}$$

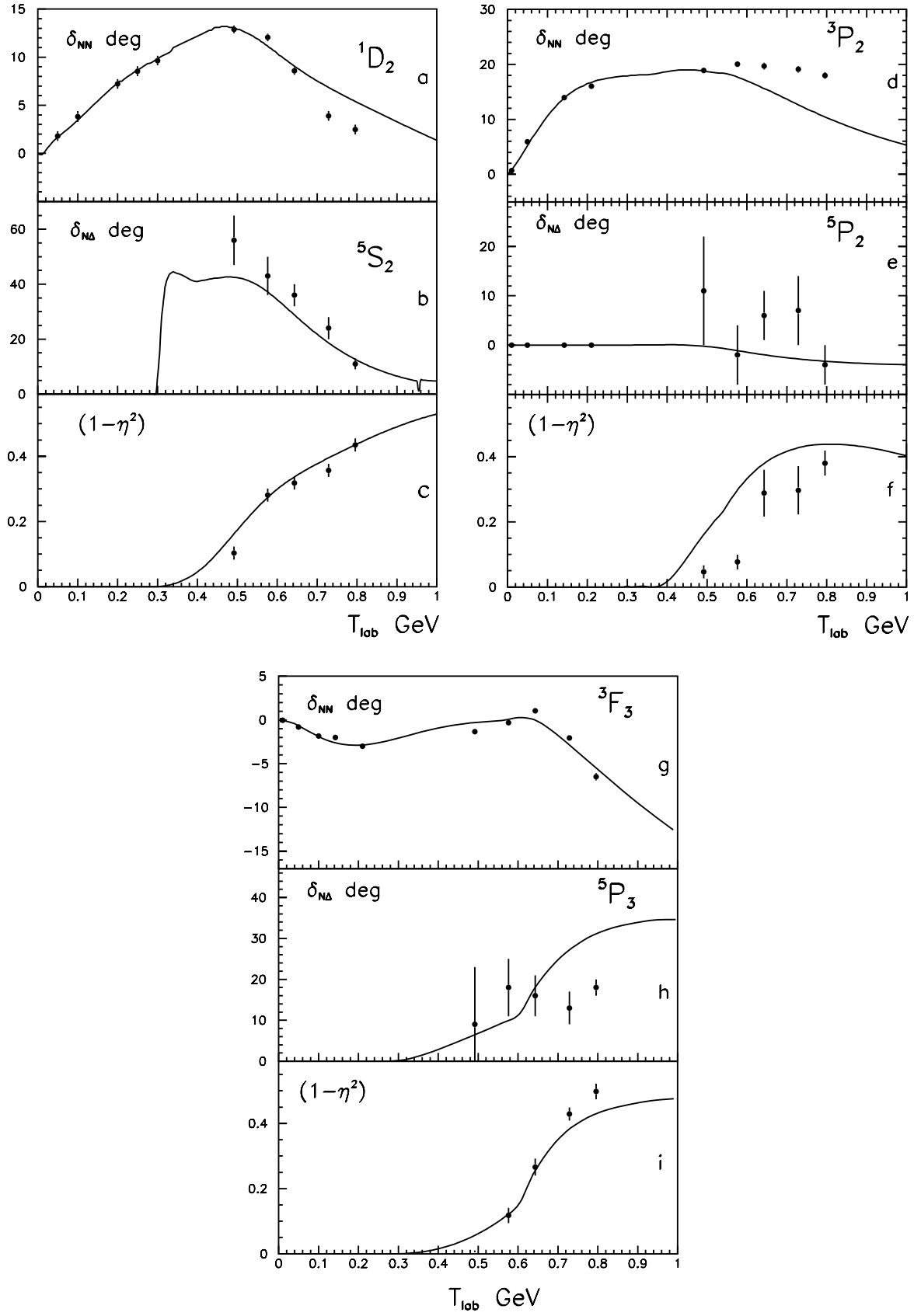

Fig. 9. Results of the fit for NN and $N\Delta$ phases and inelasticities for coupled channels ${}^1D_2(NN)-{}^5S_2(N\Delta)$ **a,b,c**, ${}^3P_2(NN)-{}^5P_2(N\Delta)$ **d,e,f**, ${}^3F_3(NN)-{}^5P_3(N\Delta)$ **g,h,i**

where the first term corresponds to the propagator of a stable particle and the second one to the propagator with the inclusion of the pion-nucleon loop diagram. The Feynman integral for the second term of the right-hand side of (2.55) is equal to:

$$\frac{(\hat{p}+M_R)}{M_R^2-p^2}\int\frac{d^4k}{(2\pi)^4 i}\frac{c_\pi^2(\hat{k}+m)}{(m^2-k^2)(m_\pi^2-(p-k)^2)}\frac{(\hat{p}+M_R)}{M_R^2-p^2}. \tag{2.56}$$

The comparison of eqs. (2.55) and (2.56) provides an expression for Γ_R^w in terms of c_π^2. To this end, let us decompose k in the external vectors p and $k^\perp$, the latter being orthogonal to p:

$$k=\alpha p+k^\perp, \tag{2.57}$$

where $\alpha=(p^2+m^2-m_\pi^2)/2p^2$. The term proportional to $k^\perp$ vanishes in (2.56). When comparing (2.55) and (2.56), it is necessary to calculate imaginary part of the loop diagram and to neglect its real part; for this purpose the following replacement should be done:

$$\frac{1}{(m^2-k^2)(m_\pi^2-(p-k)^2} \tag{2.58}$$
$$\to\frac{1}{2i}(2\pi i)^2\delta(m^2-k^2)\theta(k_0)\delta(m_\pi^2-(p-k)^2)\theta(p_0-k_0).$$

Final expression for the width Γ_R^w takes a form:

$$\Gamma_R^w=\frac{c_\pi^2}{8\pi M_R\sqrt{s}}[(M_R+m)^2-m_\pi^2]\times\left[\frac{(s+m^2-m_\pi^2)^2}{4s}-m^2\right]^{1/2}. \tag{2.59}$$

Vertex operator for the NR system in the ${}^1S_0$ state is:

$${}^1S_0(NR):\quad Q=\frac{1}{\sqrt{\Omega}}\mathbf{1},\quad \tilde{Q}=Q. \tag{2.60}$$

The description of the NN amplitude is performed within the framework of the two-channel amplitude, where the first channel is the NN-state and the second is $N\Delta$, or NN^*, or $NN\pi$ states, depending on the model we use. The amplitude is restored basing on the phase shift analysis data of [17]. The results of fitting to the phase shift analysis data for the ${}^1S_0$ wave are shown in Fig. 10a,b. All three models work equally well in the description of the experimental data on the elastic amplitude $NN\to NN$. However, they provide different results for the amplitude $NN\to NN\pi$.

2.8 $NN^*(1400)$ channel as a source of inelasticity in ${}^3P_0$ and ${}^3P_1$ waves

The description of the ${}^3P_0$ and ${}^3P_1$ NN waves is performed assuming the production of $N^*(1400)$ as a source of inelasticity in the intermediate state. The results of fitting procedure for the ${}^3P_0$ and ${}^3P_1$ waves are shown in Fig. 10c-f. Fitting parameters are given in Appendix A.

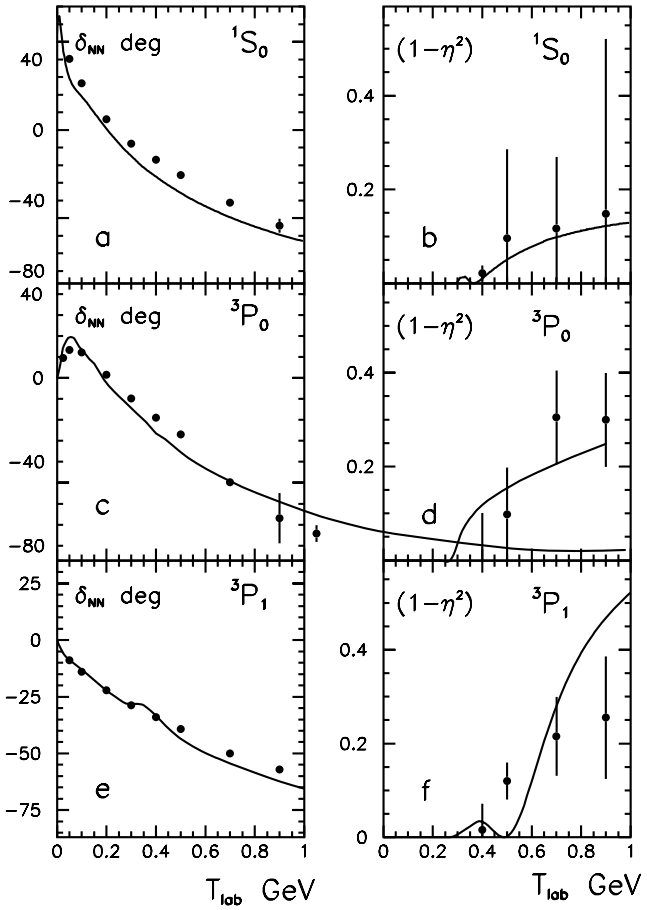

Fig. 10. Results of the fit for the phases and inelasticities in the two-channel approach for the waves ${}^1S_0$, ${}^3P_0$, ${}^3P_1$: **a** phase shifts in the wave ${}^1S_0$, δ_{NN}, **b** inelasticity in the wave ${}^1S_0$, $(1-\eta^2)$; **c** phase shifts in ${}^3P_0$, **d** inelasticity in ${}^3P_0$; **e** phase shifts in ${}^3P_1$, **f** inelasticity in ${}^3P_1$

3 Deuteron photodisintegration within the dispersion relation technique

In this Section the deuteron photodisintegration amplitude is calculated on the basis of the analysis performed in previous Section. This amplitude is represented as a sum of the pole (impulse approximation) diagram (Fig. 1a), diagram with nucleon-nucleon final state interaction (Fig. 1b) and diagrams with the photoproduction of $\Delta(1232)$, $N^*(1400)$ and pions in the intermediate state (Fig. 1c,e,f). It should be stressed that all parameters which are necessary for the calculation of these diagrams have been found in Sect. 2, where nucleon–nucleon interaction has been studied; therefore, the calculation of $\gamma d\to pn$ amplitude is parameter-free.

3.1 Pole diagram

Consider the amplitude A^{pol}, which corresponds to the pole diagram of Fig. 11a written within the dispersion relation technique. We start with the presentation of the

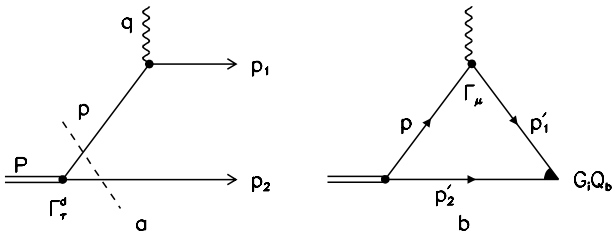

Fig. 11. Pole diagram for the deuteron disintegration **a**, triangle diagrams with nucleon **b** and Δ **c** in the intermediate state corresponding to (3.20) and (3.41)

Feynman pole diagram:

$$A^{pol} = \xi_\tau \varepsilon_\mu M^{pol}_{\tau\mu}\,, \tag{3.1}$$

where

$$M^{pol}_{\tau\mu} = \bar\Psi(p_1)\Gamma_\mu \frac{\hat p + m}{m^2 - p^2} I^d \Gamma^d_\tau \Psi_c(-p_2)\,. \tag{3.2}$$

Here ξ_τ and ε_μ are polarization vectors of the deuteron and photon which are orthogonal to the deuteron and photon, P $(P^2 = M^2)$ and q $(q^2 = 0)$, momenta:

$$(\xi P) = 0\,, \qquad (\varepsilon q) = 0\,. \tag{3.3}$$

The deuteron isotopic operator, $I^d(I = 0)$, is

$$I^d_{ij} = \frac{\delta_{ij}}{\sqrt{2}}\,. \tag{3.4}$$

Vertex functions for the transition *deuteron* $\to$ *nucleons*, Γ^d_τ, and for the photon-nucleon interaction, Γ_μ, are of the form:

$$\begin{aligned} \Gamma^d_\tau &= \gamma_\tau \phi + (p - p_2)_\tau \varphi, \\ \Gamma_\mu &= e(\gamma_\mu f_1 + (p + p_1)_\mu f_2)\,, \end{aligned} \tag{3.5}$$

where the vertex functions f_1 and f_2 are matrices in the isotopic space:

$$f_i = (f^p_i + f^n_i)\mathbf{1} + (f^p_i - f^n_i)\tau_3\,. \tag{3.6}$$

Here $\mathbf{1}$ and τ_3 are isotopic matrices $\mathbf{1} = diag(1,1)$ and $\tau_3 = diag(1,-1)$. Indices p and n stand for the photon-proton and photon-neutron form factors; ϕ, φ and $f^N_i (N = p, n)$ depend on invariant variables.

Consider the transition from the Feynman pole amplitude (3.2) to the dispersion relation one. For this diagram the dispersion relation is written in the deuteron channel, where the pole diagram contains the two-particle threshold only, which corresponds to the production of two nucleons in the intermediate state (in Fig. 11a the relevant two-particle cut is shown by dashed line).

When going from the Feynman amplitude to the dispersive one, the intermediate state vector $\tilde P$ should be introduced, see Fig. 11a: $\tilde P = p + p_2$, $\tilde P^2 = \tilde s$. The transition to the dispersive integral in the deuteron channel is carried out at fixed total energy $s = (p_1 + p_2)^2$. Let us introduce $\tilde q = -p + p_1$ which satisfies the equations:

$$\tilde P + \tilde q = p_1 + p_2 = P + q. \tag{3.7}$$

For the calculation of kinematic relations, it is suitable to use the deuteron rest frame, where

$$\begin{aligned} &q = (q_0, \boldsymbol{q}), \quad P = (M, 0), \quad \tilde P = (\sqrt{\tilde s}, 0), \\ &\tilde q = (M + q_0 - \sqrt{\tilde s}, \boldsymbol{q}). \end{aligned} \tag{3.8}$$

One can see that $\tilde q^2 = (p - p_1)^2 \neq q^2$. This inequality is related to the energy non-conservation in the dispersive integrals. The photon energy in the deuteron rest frame q_0 is determined by s as:

$$M^2 + 2Mq_0 = s. \tag{3.9}$$

We get from (3.8) and (3.9):

$$\tilde q^2 = s + \tilde s - \frac{\sqrt{\tilde s}}{M}(s + M^2). \tag{3.10}$$

The calculation of discontinuity in the deuteron channel is equivalent to the replacement of the propagator by the δ-function, considering the two-nucleon intermediate state as a real one:

$$\frac{1}{m^2 - p^2} \to \frac{1}{2}(2\pi i)\delta(m^2 - p^2)\theta(p_0)\,. \tag{3.11}$$

Using the discontinuity across the two-nucleon cut, we reconstruct the amplitude

$$\begin{aligned} M^{pol}_{\tau\mu} = \int_{4m^2}^{\infty} \frac{d\tilde s}{\tilde s - M^2} &\delta(m^2 - p^2)\theta(p_0)\bar\Psi(p_1) \\ &\times \Gamma_\mu(\hat p + m) I^d \Gamma^d_\tau(\tilde s)\Psi_c(-p_2)\,. \end{aligned} \tag{3.12}$$

The substitution (3.11) corresponds to the physical decay of virtual deuteron with the momentum $\tilde P$ into two nucleons, with the on-shell momenta p and p_2. Rewriting the δ-function argument in the form

$$p^2 - m^2 = \tilde s - 2\tilde P p_2, \tag{3.13}$$

we elimitate the integration in (3.12):

$$M^{pol}_{\tau\mu} = \frac{2}{\tilde s - M^2}\bar\Psi(p_1)\Gamma_\mu(\hat{\tilde P} - \hat p_2 + m) I^d \Gamma^d_\tau \Psi_c(-p_2)\,. \tag{3.14}$$

In the photon-deuteron center-of-mass frame one has:

$$\begin{aligned} &\tilde s = \frac{1}{4}\left(\frac{s + M^2}{M} - \sqrt{\frac{s - 4m^2}{s}}\frac{s - M^2}{M} z\right)^2, z = \cos(\boldsymbol{q}, \boldsymbol{p}_1), \\ &\tilde P = \sqrt{\frac{\tilde s}{s}}\left(\frac{s + M^2}{2M}, \boldsymbol{n}\frac{s - M^2}{2M}\right)\,. \end{aligned} \tag{3.15}$$

Compare the expressions for the pole diagram provided by the Feynman amplitude and the dispersion relation one. In the deuteron rest frame the denominator of the Feynman amplitude (3.2) is:

$$2(m^2-p^2)=2(2Mp_{20}-M^2)=2M(2p_{20}-M). \quad (3.16)$$

Corresponding denominator related to the pole term in the dispersion relation amplitude is equal to:

$$\tilde{s}-M^2=4p_{20}^2-M^2=(2p_{20}+M)(2p_{20}-M). \quad (3.17)$$

Let us stress that the momentum p is different in both techniques, namely, $p=P-p_2$ for the Feynman integral and $p=\tilde{P}-p_2$ for the dispersive one and, correspondingly, the functions ϕ,φ,f_1 and f_2 are different too. However, in the non-relativistic limit, $(2p_{20}+M)\simeq 2M$, the dispersive and Feynman pole amplitudes coincide with each other.

Since the intermediate particles in the dispersive technique are mass-on-shell, the functions ϕ and φ in (3.5) depend on $\tilde{P}^2$ only ($\tilde{P}^2=\tilde{s}$). Their numerical values are given in [21]. The form factors f_1^N and f_2^N depend on q^2 only.

These functions can be expressed in a standard way in terms of the electric, f_e^N, and magnetic, f_m^N, nucleon form factors:

$$f_1^N=f_m^N,\quad f_2^N=\frac{2m}{4m^2-q^2}(f_e^N-f_m^N)\,. \quad (3.18)$$

In (3.18) q^2 is equal to zero.

3.2 Nucleon–nucleon final state interaction

We calculate here the triangle diagram of Fig. 11b, with nucleon–nucleon interactions in the final state. In the triangle diagram the nucleonic degrees of freedom are taken into account only; contribution of non-nucleonic degrees of freedom is considered in the next Section. Although we consider here the one–channel nucleon–nucleon amplitude, the developed method can be easily generalized for the case of multichannel scattering in the final state, such as the scattering in ${}^3S_1-{}^3D_1$ waves.

We classify partial $\gamma d\to pn$ amplitudes according to the final state pn-waves (pn system in the state b is determined by (2.4) and (2.33)). The amplitude $\gamma d\to pn$ with the pn final state interaction is written as

$$A_{tr}^b=\xi_\tau\epsilon_\mu M_{\tau\mu}^b\,, \quad (3.19)$$

where

$$M_{\tau\mu}^b=\hat{g}^T(\mathbf{1}-B)^{-1}\Delta_{\tau\mu,\alpha'\beta'}(\bar{\Psi}(p_1)I_{ij}^b\tilde{Q}_{\alpha\beta}^b\Psi_c(-p_2))\,. \quad (3.20)$$

The amplitude $\Delta_{\tau\mu,\alpha\beta}$ corresponds to the triangle diagram contribution, Fig. 11b, while $M_{\tau\mu}^b$ is a sum of graphs with a full set of the final state nucleon rescattering diagrams. Vertex matrix $\hat{g}^T$ and loop diagram matrix B are determined by the pn scattering amplitude, see (2.30)–(2.34). $\Delta_{\tau\mu,\alpha'\beta'}$ can be written in the form analogous to $\hat{g}$:

$$\Delta_{\tau\mu,\alpha\beta}=\begin{pmatrix}\Delta^1_{\tau\mu,\alpha\beta}\\ \Delta^2_{\tau\mu,\alpha\beta}\\ \vdots\end{pmatrix}\,. \quad (3.21)$$

As for the calculation of the pole diagram, we start with the Feynman amplitude for $\Delta_{\tau\mu,\alpha\beta}$:

$$\Delta^i_{\tau\mu,\alpha\beta}=\int\frac{d^4p_1'}{(2\pi)^4 i} \quad (3.22)$$
$$\times\frac{-Sp(\Gamma_\tau^d I^d(\hat{p}'+m)\Gamma_\mu(\hat{p'}_1+m)G_iQ^b_{\alpha\beta}I_b(-\hat{p'}_2+m))}{(m^2-p'^2)(m^2-p_1'^2)(m^2-p_2'^2)}.$$

After summing over isotopic indices, one gets

$$Sp(I^d\Gamma_\mu I_b)=(f_1^p+(-1)^I f_1^n)\gamma_\mu+(f_2^p+(-1)^I f_2^n)(p+p_2)_\mu \equiv\tilde{\Gamma}_\mu\,. \quad (3.23)$$

To make a transition from the Feynman amplitude (3.22) to the dispersion relation one, it is necessary to carry out the following steps:

1. To expand the numerator of (3.22) in external four–vectors, for which we choose P and $P_f=p_1'+p_2'$:

$$-Sp\,(\Gamma_\tau^d I^d(\hat{p}'+m)\tilde{\Gamma}_\mu(\hat{p'}_1+m)G_iQ^b_{\alpha\beta}I^b(-\hat{p'}_2+m)) =\sum_j d_j^i F^j_{\tau\mu,\alpha\beta}\,. \quad (3.24)$$

Here $F^j_{\tau\mu,\alpha\beta}$ is an expression built up from the vectors P,P_f and tensors $g_{\tau\mu},\varepsilon_{\mu\tau\alpha\beta}$. The procedure for constructing invariant functions d_j^i and the explicit form of $F^j_{\tau\mu,\alpha\beta}$ for various pn scattering channels is given in [38].

2. Using (3.24), to represent the expression for $\Delta^i_{\tau\mu,\alpha\beta}$ in the form:

$$\Delta^i_{\tau\mu,\alpha\beta}=\sum_j D_j^i F^j_{\tau\mu,\alpha\beta}\,. \quad (3.25)$$

For the presentation of D_j^i as dispersion relation amplitudes, the double discontinuity of the triangle diagram is calculated, i.e. the intermediate two-particle state is considered as a real one, with the neutron–proton energy $\sqrt{\tilde{s}}$ before and $\sqrt{s'}$ after the interaction ($\tilde{s},s'\geq 4m^2$). This procedure corresponds to the replacement:

$$\frac{1}{(m^2-p'^2)(m^2-p_1'^2)(m^2-p_2'^2)} \to\frac{1}{4}(2\pi i)^3\delta(m^2-p'^2)\theta(p_0') \quad (3.26)$$
$$\times\delta(m^2-p_1'^2)\theta(p_{10}')\delta(m^2-p_2'^2)\theta(p_{20}')\equiv\rho(\tilde{s},s',z)\,.$$

3. To reconstruct the function D_j^i using the dispersion integral with a double discontinuity as an integrand:

$$D_j^i=\int_{4m^2}^\infty\frac{d\tilde{s}\;ds'}{\pi^2}\frac{disc\;disc\,D_j^i}{(\tilde{s}-M^2)(s'-s)}\,. \quad (3.27)$$

Here

$$disc\ discD^i_j = \int \frac{d^4p_1}{(2\pi)^4}\rho(\tilde{s},s',z)d^i_j(\tilde{s},s',z)\,. \qquad (3.28)$$

Using the results obtained by the derivation of (3.14), we integrate over s in (3.27). This gives:

$$D^i_j = \int \frac{ds'}{\pi}\int_{-1}^{1}\frac{dz}{2}\rho(s')\frac{2d^i_j(\tilde{s},s',z)}{(\tilde{s}-M^2)(s'-s)}\,. \qquad (3.29)$$

$\rho(s')$ is given by (2.7), $\tilde{s}$ is defined according to (3.15), $s = P_f^2$, $z = \cos(\boldsymbol{q},\boldsymbol{p'}_1)$. Invariant functions D^i_j determine the function $\Delta_{\tau\mu,\alpha\beta}$ (3.25) and, consequently, the amplitude $M^b_{\tau\mu}$.

3.3 Photodisintegration amplitude with $\Delta(1232)$ in the intermediate state

In this Section we include Δ-isobar produced in the intermediate state into the photodisintegration amplitude. The importance of the isobar in the deuteron photodisintegration was emphasized in numerous papers (see, for example, [33], [34], [36]). The isobar reveals itself in two ways:

1) As $N\Delta$ intermediate state in the final nucleon-nucleon rescatterings (dashed block in Fig. 1b,c);

2) In the prompt photoproduction, with a subsequent transition $N\Delta \to pn$ in the triangle diagrams of Fig. 1e-type.

Here we calculate the photodisintegration amplitude with $N\Delta(1232)$ in the intermediate state, taking into account the coupled channels ${}^1D_2(NN)$ $-{}^5S_2(N\Delta)$, ${}^3P_2(NN)$ $-{}^5P_2(N\Delta)$, and ${}^3F_3(NN)$ $-{}^5P_3(N\Delta)$.

1) **Δ-isobar, γN partial width and the coupling**

We start the treatment of $\Delta(1232)$ in the deuteron photoproduction amplitude with a consideration of the transition coupling for $N\gamma \to \Delta$, which determines the process of Fig. 1e. The propagator of the stable Δ-isobar, with mass m_Δ, is equal to

$$\frac{(\hat{p}+m_\Delta)(-g^\perp_{\alpha\beta}+\frac{1}{3}\gamma^\perp_\alpha\gamma^\perp_\beta)}{m^2_\Delta - p^2}\,. \qquad (3.30)$$

Re-definition of the propagator, for the case of the decay into nucleon and photon, consits in the replacement:

$$(m^2_\Delta - p^2)^{-1} \to (m^2_\Delta - p^2 - B_\gamma(p^2))^{-1}\,, \qquad (3.31)$$

where $B_\gamma(p^2)$ is the photon–nucleon loop diagram. Real part of this diagram re-determines m_Δ, and the imaginary part of $B_\gamma(p^2)$ gives partial width Γ^w_γ for the decay $\Delta \to \gamma N$:

$$\frac{(\hat{p}+m_\Delta)(-g^\perp_{\alpha\beta}+\frac{1}{3}\gamma^\perp_\alpha\gamma^\perp_\beta)}{m^2_\Delta - p^2 - im_\Delta\Gamma^w_\gamma(p^2)}\,. \qquad (3.32)$$

Thus, we have to calculate $B_\gamma(p)$. The following expression stands for the Δ-isobar propagator with $B_\gamma(p)$ considered as a perturbative correction:

$$\frac{(\hat{p}+m_\Delta)(-g^\perp_{\alpha'\beta}+\frac{1}{3}\gamma^\perp_{\alpha'}\gamma^\perp_\beta)}{m^2_\Delta - p^2} \times \int \frac{d^4q}{(2\pi)^4 i}\,\Gamma^\Delta_{\alpha\mu}\,\frac{(\hat{k}+m)}{m^2-k^2}\,\Gamma^\Delta_{\beta\mu'}\,\frac{g_{\mu\mu'}}{-q^2} \times \frac{(\hat{p}+m_\Delta)(-g^\perp_{\alpha\beta'}+\frac{1}{3}\gamma^\perp_\alpha\gamma^\perp_{\beta'})}{m^2_\Delta - p^2}\,. \qquad (3.33)$$

The vertex operator $\Gamma^\Delta_{\alpha\mu}$ has the form [45]:

$$\Gamma^\Delta_{\alpha\mu} = c_\gamma\gamma_5(\hat{q}g_{\mu\alpha} - q_\alpha\gamma_\mu)\sqrt{2}T_0\,. \qquad (3.34)$$

Let us decompose the vectors k and q in vectors p and $k^\perp$ ($k^\perp$ is orthogonal to p):

$$q = Ap + k^\perp\,, \qquad k = Bp - k^\perp\,, \qquad (3.35)$$

where

$$A = \frac{p^2 - m^2_\Delta}{2p^2}\,, \qquad B = \frac{p^2+m^2_\Delta}{2p^2}\,.$$

To calculate the imaginary part of (3.33) the following replacement should be done:

$$\frac{1}{(-q^2)(m^2-k^2)} \to \frac{1}{2}(2\pi i)^2\delta(m^2-k^2)\theta(k_0)\delta(-q^2)\theta(q_0)\,. \qquad (3.36)$$

When integrating over $k^\perp$, the terms proportional to $k^\perp$ and $k^{\perp 3}$ vanish, while the quadratic terms should be replaced as follows:

$$k^\perp_\alpha k^\perp_\beta \to \frac{1}{3}\left[-\frac{(p^2-m^2)}{4p^2}\right]g^\perp_{\alpha\beta} = \frac{1}{3}k^2_\perp g^\perp_{\alpha\beta}\,. \qquad (3.37)$$

Using the equality

$$\left(-g^\perp_{\alpha\beta}+\frac{1}{3}\gamma^\perp_\alpha\gamma^\perp_\beta\right)\left(-g^\perp_{\beta\varepsilon}+\frac{1}{3}\gamma^\perp_\beta\gamma^\perp_\varepsilon\right) = \left(-g^\perp_{\alpha\varepsilon}+\frac{1}{3}\gamma^\perp_\alpha\gamma^\perp_\varepsilon\right).$$

one obtains:

$$\frac{(\hat{p}+m_\Delta)(-g^\perp_{\alpha'\beta'}+\frac{1}{3}\gamma^\perp_{\alpha'}\gamma^\perp_{\beta'})}{m^2_\Delta - p^2}\hat{p}\left(A^2Bp^2 - \frac{2}{3}Ak^2_\perp - \frac{1}{3}Bk^2_\perp\right) \times i\frac{p^2-m^2}{16\pi m_\Delta p^{1/2}}\,c^2_\gamma\,. \qquad (3.38)$$

Fixing $p^2 = m^2_\Delta$ in the numerator, we have for the width Γ^w_γ:

$$\Gamma^w_\gamma = \frac{1}{8\pi}\left(\frac{m^2_\Delta - m^2}{2m_\Delta}\right)^3\frac{2m^2_\Delta + \frac{2}{3}m^2}{m^2_\Delta}\,c^2_\gamma\,. \qquad (3.39)$$

After presenting c_γ as $c_\gamma = (e/m_\pi)C$, we get $C = 0.30$ (at $\Gamma^w_\gamma/\Gamma^w_{tot} = 0.006$ and $\Gamma^w_{tot} = 115$ MeV), in accordance with [46] and [34].

2) ***pn*-production in the waves ${}^1D_2(NN)$, ${}^3P_2(NN)$ and ${}^3F_3(NN)$**

The amplitude of the process $\gamma d \to pn$ is given by (3.20). For the waves ${}^1D_2(NN)$, ${}^3P_2(NN)$ and ${}^3F_3(NN)$), the structure of the triangle diagram $\hat{\Delta}_{\tau\mu,\alpha\beta}$ is the same as $\hat{g}$ given by (2.48), namely:

$$\hat{\Delta} = \begin{bmatrix} \Delta^N & 0 \\ \Delta^t & 0 \\ 0 & \tilde{\Delta}^r \\ 0 & \tilde{\Delta}^\Delta \end{bmatrix} . \qquad (3.40)$$

We have two types of triangle diagrams: with nucleons in the intermediate state, Δ^N and Δ^t (Fig. 11b), and with $N\Delta$ intermediate state, $\tilde{\Delta}^r$ and $\tilde{\Delta}^\Delta$ (Fig. 11c). The calculation of Δ^i is given in Section 3.2. The scheme of calculation of $\tilde{\Delta}^i$ is presented below. The Feynman integral corresponding to the diagram of Fig. 11c is:

$$\tilde{\Delta}^i_{\tau\mu,\alpha\beta} = \int \frac{d^4p'_1}{(2\pi)^4 i} \qquad (3.41)$$
$$\frac{-Sp(\Gamma^d_\tau \tilde{I}^d(\hat{p'}+m)\Gamma^\Delta_{\mu\varepsilon}(\hat{p'}_1+m_\Delta)\tilde{P}_{\varepsilon\varepsilon'}G_i Q^a_{\alpha\beta,\varepsilon'}T_0(-\hat{p}'_2+m))}{(m^2-p'^2)(m^2_\Delta-p'^2_1)(m^2-p'^2_2)},$$

where $\Gamma^\Delta_{\mu\varepsilon}$ is the vertex for the Δ-photoproduction (3.34). The spin-dependent numerator of the isobar propagator $\tilde{P}_{\varepsilon\varepsilon'}$ is:

$$\tilde{P}_{\varepsilon\varepsilon'} = -g^\perp_{\varepsilon\varepsilon'} + \frac{1}{3}\gamma^\perp_\varepsilon \gamma^\perp_{\varepsilon'} , \qquad (3.42)$$

where

$$g^\perp_{\varepsilon\varepsilon'} = g_{\varepsilon\varepsilon'} - \frac{p'_{1\varepsilon}p'_{1\varepsilon'}}{p'^2_1} , \qquad \gamma^\perp_\varepsilon = \gamma_\varepsilon - \frac{\hat{p'}_1 p'_{1\varepsilon}}{p'^2_1} .$$

The expression (3.41) is written for a stable isobar. In the case of an unstable isobar decaying into pion and nucleon, the pole term should be replaced as:

$$(m^2_\Delta - p'^2_1)^{-1} \to (m^2_\Delta - p'^2_1 - B_\pi(p'^2_1))^{-1} ,$$

where the function $B_\pi(p'^2_1)$ is determined by the pion–nucleon loop diagram. The real part of this diagram redetermines the mass, and the imaginary part gives the width Γ^w_π of the decay $\Delta \to N\pi$:

$$Im\, B_\pi(p'^2_1) = m_\Delta \Gamma^w_\pi(p'^2_1) .$$

Using the Lehman representation, the isobar propagator can be written as follows:

$$(m^2_\Delta - p'^2_1 - i m_\Delta \Gamma^w_\pi(p'^2_1))^{-1} = \int_{(m+m_\pi)^2}^\infty \frac{d\tilde{m}^2 R(\tilde{m}^2)}{\tilde{m}^2 - p'^2_1 - i0} ,$$

where the weight function $R(\tilde{m}^2)$ is of the form:

$$R(\tilde{m}^2) = \frac{1}{\pi}\frac{m_\Delta \Gamma^w_\pi(\tilde{m}^2)}{(m^2_\Delta - \tilde{m}^2)^2 + (m_\Delta \Gamma^w_\pi(\tilde{m}^2))^2} . \qquad (3.43)$$

Below we accept $\Gamma^w_\pi = \Gamma^w_{tot}$, and the parametrization of ref. [33] is used for the momentum-dependent width:

$$\Gamma^w_\pi(\tilde{m}^2) = \Gamma^w_{tot}\frac{\tilde{X}^3/(1+\tilde{X}^2)}{X^3_\Delta/(1+X^2_\Delta)} ,$$

Here $\tilde{X} = \tilde{q}r/m_\pi$, $X_\Delta = q_\Delta r/m_\pi$ with r=0.081, $\tilde{q}$ and q_Δ are pion momenta in the isobar center-of-mass frame for the isobar masses $\tilde{m}$ and m_Δ, correspondingly.

Transition from the Feynman amplitude (3.41) to the dispersion relation one makes it necessary to follow the prescription given in Sect. 3.2. Then we get for D^i_j:

$$D^i_j = \int_{(m+m_\pi)^2}^\infty d\tilde{m}^2 R(\tilde{m}^2) \int_{(m+\tilde{m})^2}^\infty \frac{ds'}{\pi} \times \int_{-1}^1 \frac{dz}{2}\frac{2d^i_j}{(\tilde{s}-M^2)(s'-s_f)} \times \left(\frac{(s'-(\tilde{m}+m)^2)(s'-(\tilde{m}-m)^2)}{s'^2}\right)^{1/2}\frac{1}{16\pi}. \qquad (3.44)$$

3.4 Deuteron photodisintegration and inelasticities in the final state waves ${}^1S_0$, ${}^3P_0$ and ${}^3P_1$

In Sects. 2.7–2.8 the description of NN scattering in the waves ${}^1S_0$, ${}^3P_0$ and ${}^3P_1$ has been done, with three different models suggested for the mechanism of inelasticity: production of $\Delta(1232)$, $N^*(1440)$, or $(\pi N)_S$-pair. It is shown in Appendix A that the transition amplitude $NN \to NN$ does not depend on the model used for the inelasticity, i.e. on the type of the transition amplitude $NN \to NR$, $NR \to NN$ and $NR \to NR$, where $R = \Delta, N^*$, or $(\pi N)_S$.

This means that the process of Fig. 1b does not depend on the inelasticity type as well, and it may be calculated within the technique presented in Sect. 2. However, the processes of Fig. 1c,e,f, with a prompt photoproduction of a resonance or pion–nucleon pair, may depend on the inelasticity type. For the calculation of processes of Fig. 1c,e,f, it is necessary to know the resonance photoproduction amplitudes. It should be noted that $N^*(1400)$ has an about 50% branching rate into the channel $N\pi\pi$, so the triangle diagram with $N^*(1400)$ in the intermediate state effectively describes the process of Fig. 1d.

1) **Triangle diagram with $N\Delta$ intermediate state**

The vertex $\gamma N \to \Delta$ has been presented in Sect. 3.3. The calculation of triangle diagram with $N\Delta$ intermediate state is carried out in the same way as for the waves considered in previous Section.

2) **Triangle diagram with $NN^*(1400)$ intermediate state**

The resonance $N^*(1440)$ has the same quantum numbers as a nucleon, $J^p = \frac{1}{2}^+$, and the vertex function F_γ for the transition $N\gamma \to N^*$ is equal to:

$$\Gamma^{N^*}_\mu = c_\gamma \gamma_\mu \tau_3 , \qquad (3.45)$$

with the following relation between c_γ and the width Γ^w_γ of the decay $N^* \to \gamma N$:

$$\Gamma^w_\gamma M_{N^*} = c^2_\gamma \frac{2(M_{N^*}-m)^2}{16\pi M^2_{N^*}}(M^2_{N^*}-m^2) . \qquad (3.46)$$

The correlation between Γ^w_γ and c_γ may be found in the same way as it has been done in previous Section for

$\Delta(1232)$. To define c_γ, we rely upon the fact that the total width of N^* is equal to $\Gamma_{tot} = 200$ MeV. Let the ratio $\Gamma^w_\gamma/\Gamma^w_{tot}$ be the same for $p\gamma$ and $n\gamma$ channels, being equal to 0.10% [46]. Using (3.46), we get $c_\gamma = 0.3$. Experimental data [46] on N^* do not allow to define the coupling with higher accuracy.

3) **Triangle diagram with $N(\pi N)_S$ intermediate state**

Following the model presented in Sect. 2.7, we approximate pion–nucleon pair by the quasi-resonance R. Then the vertex function for the transition $\gamma N \to R$ can be written in the form:

$$\Gamma^R_\mu = c^R_\gamma \gamma_\mu \gamma_5 \tau_3 \,. \tag{3.47}$$

The coupling c^R_γ is found by calculating the $\gamma p \to \pi^+ n$ cross section:

$$\begin{aligned}\sigma(\gamma p \to \pi^+ n) = &\int_{-1}^{1} dz \frac{1}{4J}\frac{1}{16\pi s_{\gamma p}} \\ &\times [(s_{\gamma p} - (m^2_\pi + m^2))^2 - 4m^2 m^2_\pi]^{1/2} \\ &\times \frac{c^2_\pi c^2_\gamma}{(M^2_R - s_{\gamma p})^2 + M^2_R \Gamma^{w\,2}_R} g^{\perp\perp}_{\mu\mu'} \\ &\times Sp\{(\hat{k} + m)\gamma_\mu \gamma_5 (\hat{k} + \hat{k}_\pi + M_R) \\ &\times (\hat{k} + m)\gamma_{\mu'} \gamma_5 (\hat{k} + \hat{k}_\pi + M_R)\}\frac{2}{3} \,, \end{aligned} \tag{3.48}$$

where q and k are photon and neutron momenta, $s_{\gamma p}$ is the γp energy squared, and

$$\begin{aligned} &J = 2(s - m^2) \,, \quad g^{\perp\perp}_{\mu\mu'} = g_{\mu\mu'} - \frac{k_\mu k_{\mu'}}{k^2} - \frac{q^\perp_\mu q^\perp_{\mu'}}{q^{\perp 2}} \,, \\ &q^\perp_\mu = q_\mu - k_\mu \frac{(qk)}{m^2} \,. \end{aligned}$$

Parameters c_π, M_R and Γ_R standing for the quasi-resonance are introduced in Sect. 2.7. According to [47], the $\gamma p \to \pi^+ n$ cross section has a resonance pick related to the Δ-isobar and a smooth background. We relate this background to the quasi resonance production of the $(\pi N)_S$-pair. The quasi-resonance width Γ^w_R is calculated with the simplest ansatz about the vertex of the decay $R \to \pi N$:

$$\Gamma_\pi = c_\pi \boldsymbol{\tau} \,. \tag{3.49}$$

The fit provides the following parameters $c_\gamma = 0.5$, $c_\pi = 0.7$, $M_R = 1.85$ GeV.

For all considered waves ($^1S_0$, $^3P_0$ and $^3P_1$) and for all types of the models, the result is the following: processes with inelastic production in the triangle-graph intermediate state provide small contribution, in other words, the contribution of diagrams 1c, 1e and 1f is not large, while the main one comes from the diagram of Fig. 1b. For example, the maximum value of the triangle graph contribution in the wave $^1S_0$ comes at $E_\gamma = 30 - 50$ MeV, and it does not exceed 5% of $\sigma(^1S_0)$ (see below).

4 Results and discussion

4.1 Polarization averaging and cross section calculations

Within the used normalization, the differential unpolarized cross section has the form:

$$d\sigma = \frac{|A|^2}{J} d\Phi \,, \tag{4.50}$$

where A is the whole disintegration amplitude, which is built up of the amplitude $A = A^{pole} + \sum_b A^b_{tr}$ by averaging over the spins of incident particles and summed over spins of final particles. The summation $\sum_b$ is performed over all considered states $^1S_0$, $^3S_1 - ^3D_1$, $^3P_0$, $^1P_1$, $^3P_1$, $^3P_2$, $^1D_2$, $^3D_2$ and $^3F_3$.

The two-particle phase space factor, $d\Phi$, and the flux factor J are defined as:

$$\begin{aligned} d\Phi = &\frac{d^4 p_1 d^4 p^2}{(2\pi)^6}(2\pi)^4 \delta^4(P - p_1 - p_2) \\ &\times \delta(m^2 - p^2_1)\delta(m^2 - p^2_2) \,, \\ J = &\, 4((Pq)^2 - m^4)^{1/2} \,. \end{aligned} \tag{4.51}$$

For non-polarized deuteron we need to make the replacement:

$$\xi_\tau \xi_{\tau'} \to -\frac{1}{3} g^\perp_{\tau\tau'} = -\frac{1}{3}\left(g_{\tau\tau'} - \frac{P_\tau P_{\tau'}}{P^2}\right) . \tag{4.52}$$

For the non-polarized photon, it is necessary to average over the two polarization states:

$$\varepsilon_\mu \varepsilon_{\mu'} \to -\frac{1}{2} g^{\perp\perp}_{\mu\mu'} = -\frac{1}{2}\left(g_{\mu\mu'} - \frac{P_\mu P_{\mu'}}{P^2} - \frac{q^\perp_\mu q^\perp_{\mu'}}{q^{\perp 2}}\right) , \tag{4.53}$$

where $q^\perp = q - P(Pq)/P^2$, and $q_\mu g^{\perp\perp}_{\mu\mu'} = 0$ and $g^{\perp\perp}_{\mu\nu} g^{\perp\perp}_{\nu\xi} = g^{\perp\perp}_{\mu\xi}$. It means that the combination $g^{\perp\perp}_{\mu\mu'} A_{\mu'}$ which is used for the calculation of the cross section is gauge invariant.

4.2 Photodisintegration cross section: nucleonic degrees of freedom

At the first stage of our investigations [38], we have calculated the amplitude $\gamma d \to pn$ taking into account nucleonic degrees of freedom only: photodisintagration amplitude is described by the sum of diagrams 1a and 1b and the parameters of G functions are restored using the phases of NN scattering only.

Figure 12a presents the calculation result obtained in such approximation: dashed line stands for the pole diagram contribution (Fig. 1a), while solid one describes the cross section $\sigma(\gamma d \to pn)$ calculated with both diagrams 1a and 1b.

One can see that for nucleonic degrees of freedom the photodisintegration reaction is successfully described at $E_\gamma \le 10$ MeV only, in agreement with the result of [31,37].

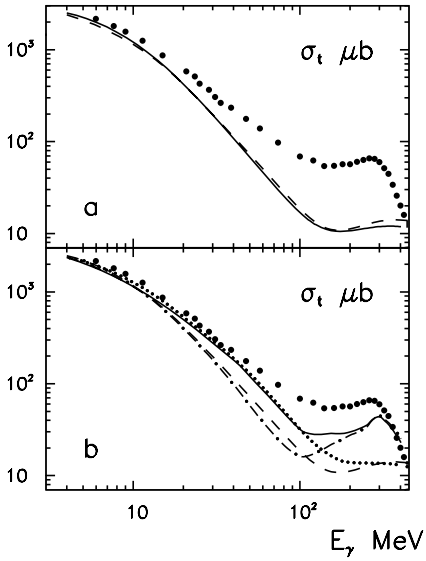

Fig. 12. Total cross section, σ_t, for the deuteron photodisintegration: **a** contribution of the impulse approximation diagram 1a to the σ_t (*dashed line*), σ_t with FSI (nucleon degrees of freedom) (*solid line*); **b** contribution of the impulse approximation diagram (*dashed line*); σ_t with the inelasticity in the waves ${}^1D_2(NN)$, ${}^3P_2(NN)$, ${}^3F_3(NN)$ (*dot-dashed line*); σ_t with the inelasticity in the waves ${}^1S_0(NN)$, ${}^3P_0(NN)$, ${}^3P_1(NN)$ (*small-dot line*); the complete σ_t (*solid line*). Experimental data [1-8] are shown by *large dots*. E_γ is the photon energy in lab. system

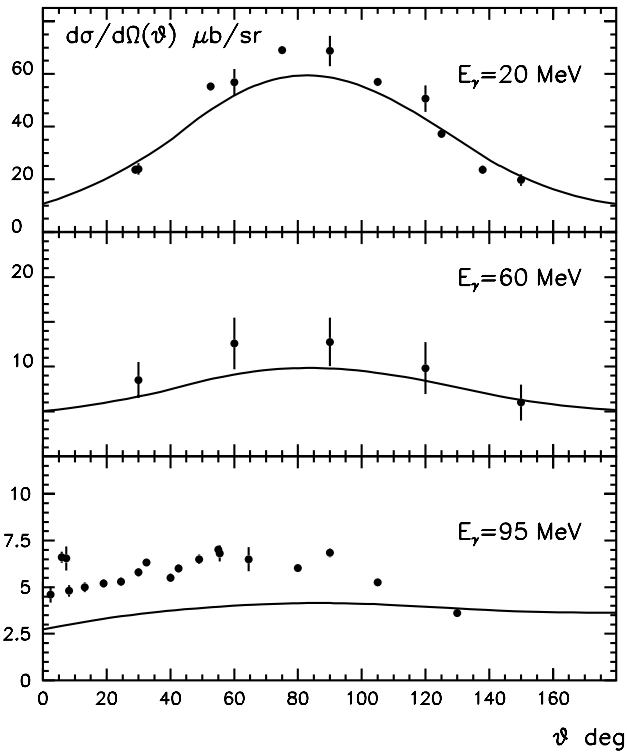

Fig. 13. Differential cross sections $d\sigma/d\Omega(\theta)$ at $E_\gamma = 20$ MeV, $E_\gamma = 60$ MeV, $E_\gamma = 95$ MeV, together with experimental data [9-13]

One should note that the diagram of final state interaction does not change the result obtained in the framework of the impulse approximation. This is a consequence of the completness condition for two sets of wave functions: plain waves and those with the *pn* interaction. The proximity of solid and dashed lines is a criterion of self-consistency of our calculations. It should be noted that in the region of very small E_γ the situation changes: the diagrams of Fig. 1a and 1b cancel each other, due to the orthogonality of the deuteron wave function and the wave function of continuous spectrum.

4.3 Contribution of inelastic channels

Inelastic processes are important in the waves ${}^3P_2$, ${}^1D_2$ and ${}^3F_3$ (the production of Δ-isobar) and in the waves ${}^1S_0$, ${}^3P_0$ and ${}^3P_1$ (the production of $N^*(1400)$ or $(\pi N)_S$-state).

The calculation result for $\sigma(\gamma d \to pn)$, with the account of inelasticities in the waves ${}^3P_2$, ${}^1D_2$ and ${}^3F_3$, is shown in Fig. 12b (dashed-dotted line). At $E_\gamma \simeq 300$ MeV the calculated cross section has a bump, but it is lower than the experimental one. At $10 \le E_\gamma \le 100$ MeV the dashed-dotted line is located below the curve which is given by the pole diagram, that is due to the destructive interference. It should be noted that in these waves the main contribution comes from the diagram of the prompt Δ-isobar production (Fig. 1e), i.e. from the process $\gamma N \to N\Delta$.

Inelasticities in the waves ${}^1S_0$, ${}^3P_0$ and ${}^3P_1$ lead to the considerable increase of the cross section $\sigma(\gamma d \to pn)$ $10 \le E_\gamma \le 200$ MeV: because of that, the cross section $\sigma_{calc}(\gamma d \to pn)$ satisfactorily describes the experimental data up to $E_\gamma \sim 60$ MeV (solid curve in Fig. 12b).

Figure 13 demonstrates the calculation results and the experimental data [10-13] for differential cross sections at $E_\gamma = 20, 60, 90$ MeV. An agreement is seen at $E_\gamma = 20, 60$ MeV. However in the region $E_\gamma > 60$ MeV there is no agreement with experimental data. One may believe that this discrepancy is due to meson currents which are not completely taken into account in our calculation.

Let us discuss in more detail the structure of processes taken and not taken into account in the approach under discussion. In terms of the analytic structure of the amplitude $\gamma d \to pn$, the diagrams with rescatterings do take into account the (s,t) and (s,u) anomalous (Landau) singularities (remind that $t = (q - p_1)^2$ and $u = (q - p_2)^2$). Figures 14a,b give an example of diagrams with such singularities: Fig. 14a demonstrates the diagram with the Landau singularity in (s,t)-sector, while the diagram of Fig. 14b has the Landau singularity in (u,t)-sector. Both these diagrams have also singularities of triangle diagrams, which are shown in Fig. 14c,d — these diagrams come to being due to the shrinkage of the upper nucleon line into a point. The diagrams of Fig. 14c–type have anomalous singularity of the logarithm type at $t \simeq m^2 + 2\mu^2 + 4\mu\sqrt{m\epsilon} \equiv t_{tr}$, that is rather close to the physical region of the reaction (ϵ is deuteron binding energy). Similarly, the singularity at $u = t_{tr}$ is inherent to the diagram of Fig. 14d. With final state interaction accounted for in our approach, we also take these sin-

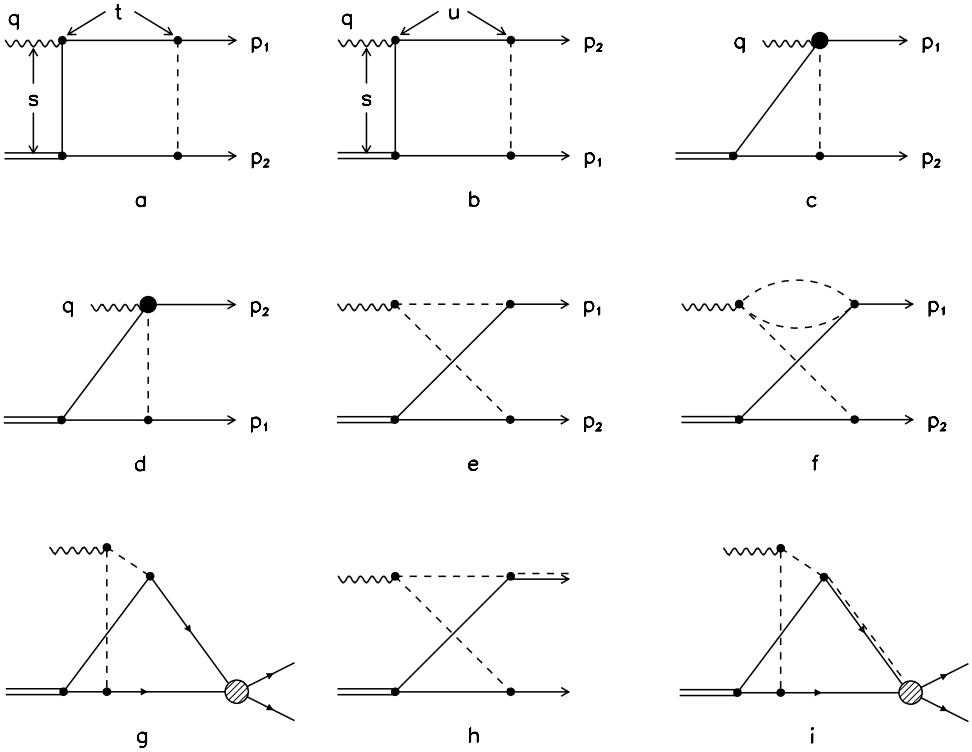

Fig. 14. Diagrams contributing to meson exchange currents, see text

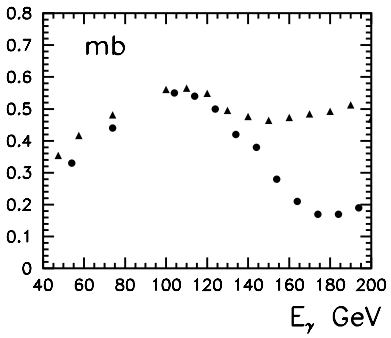

Fig. 15. Evaluation of meson exchange currents: *dotted curve* stands for the difference $\Delta\sigma = \sigma_{exp}(\gamma d \to pn) - \sigma_{calc}(\gamma d \to pn)$ obtained in our calculations and *triangles* show the contribition of Fig. 14d calculated in [31]

gularities into consideration, but not completely, for just the same diagrams are present in the (u,t)-box diagrams — see Fig. 14e,f. These latter are in fact the meson exchange current diagrams which are not included into our approach, and one may believe that the deficiency of the cross section description at $E_\gamma > 50$ MeV should be compensated with these diagrams, together with a subsequent final state interaction (Fig. 14g).

The role of meson exchange currents in the deuteron photodisintegration has been estimated by Laget [31]. Figure 15 demonstrates the difference $\Delta\sigma = \sigma_{exp}(\gamma d \to pn) - \sigma_{calc}(\gamma d \to pn)$ obtained in our calculations and the evaluation of meson exchange current contribution given in [31] for the processes shown in Fig. 14e,f. One can see that the estimation given in [31] provides a reasonable description for $\Delta\sigma$ in the region $E_\gamma = 50 - 200$ MeV but cannot explain the data at $E_\gamma \sim 300$ MeV. This is exactly the region where the bump in the cross section corresponds to the Δ isobar in the intermediate state (see Fig. 1c). Therefore, it is natural to suggest that in the considered case we meet analogous situation: the Δ isobar is produced in the process induced by meson exchange currents — see Fig. 14h. The next transition $\Delta N \to NN$ (Fig. 14i) would provide a contribution affecting the enhancement of the cross section around $E_\gamma \sim 300$ MeV. We believe that this is the only reasonable explanation of the discrepancy observed in this region: the bump in the cross section is undoubtedly due to the $N\Delta$ channel, and the only one which is not accounted for in our approach is the contribution of the (u,t) singularity into the amplitude $\gamma d \to N\Delta$, i.e. the contribution of meson currents into the process $\gamma d \to N\Delta$.

5 Conclusion

We have carried out the dispersion relation analysis of the nucleon–nucleon scattering and deuteron photodisintegration amplitudes. As a result, all the waves which are not small in the region $T_{lab} < 1$ GeV are included within the despersion N/D representation. N-functions which are the analogues of a potential are restored for the waves $^1S_0$, $^3S_1 - ^3D_1$, $^3P_0$, $^1P_1$, $^3P_1$, $^3P_2$, $^1D_2$, $^3D_2$ and $^3F_3$ (N-functions for the deuteron channel $^3S_1$ and $^3D_1$ were found before, in [21]). Besides, the N/D representation is written for inelastic amplitudes $NN \to N\Delta$ (the waves $^1D_2(NN) - ^5S_2(N\Delta)$, $^3P_2(NN) - ^5P_2(N\Delta)$ and $^3F_3(NN) - ^5P_3(N\Delta)$) and $NN \to N(N\pi)_{S-wave}$ (the

waves $^1S_0$, $^3P_0$ and $^3P_1$), thus giving a complete dispersion relation representation of the low and intermediate energy amplitude at $T < 1$ GeV.

The amplitude of the photodisintegration $\gamma d \to pn$ has been analysed in the framework of the dispersion relation technique for $E_\gamma < 400$ MeV. The spectator mechanism of the photodisintegration related to the interaction of photon with one of the deuteron nucleons is considered, the inelasticity related to the production of Δ, N^* or $(\pi N)_S$ pair being included. Furthermore, using the constructed nucleon–nucleon amplitudes, the final state interaction is properly taken into account within the dispersion relation technique. All these calculations are parameter–free, the necessary characteristics of the nucleon-nucleon amplitude are directly taken from the experiment, that is, γN amplitudes, deuteron vertices found in [21] from the fit of the deuteron form factors at $Q^2 \leq 1.5$ (GeV/c)^2 and the NN amplitudes found in this paper. Using the language of the dispersion relation representation, meson exchange currents are the contributions of the (u,t)-singular part of the amplitude $A(\gamma d \to pn)$. The performed calculations allow one to evaluate meson exchange current contribution: the difference between the observed and calculated cross sections is a direct measure of it. The analysis shows that the spectator mechanism for the photon-deuteron interaction, with a consistent account of final state interaction, adequately describes the data at $E_\gamma < 50$ MeV. However, at $E_\gamma > 50$ MeV the meson exchange currents begin to dominate, providing more than a half of the cross section at $E_\gamma \geq 100$ MeV. Comparing the results of our calculations with those of Laget [31], one may conclude that the standard mechanism for meson current contribution, namely, the interaction of incident photon with a meson which provides an exchange between deuteron nucleons, may explain the value of the deuteron photodisintegration cross section at $E_\gamma < 150$ MeV only, but not around 300 MeV. It favours the idea that the bump in $\sigma_{tot}(\gamma d \to pn)$ at $E\gamma \simeq 300$ MeV, with the width about 300 MeV, is due to the contribution of the (u,t)-singular part of the amplitude $\gamma d \to N\Delta$, that is just the meson exchange current contributing into $NN \to N\Delta$ when the photon interacts with t- or u-channel meson.

At the same time, our analysis gives rise to the problem of meson exchange currents in the deuteron channel (NN $^3S_1$ and $^3D_1$ waves): the matter is that deuteron form factors $A(Q^2)$ and $B(Q^2)$ are well described in a broad interval, $0 < Q^2 \leq 1.5$ (GeV/c)^2, without an exchange current [21]. It is possible that in this respect the deuteron channel is a singular one, and meson exchange currents are not large there. It is well-known that in the deuteron channel the inelasticities are strongly suppressed: we cannot exclude that in the deuteron channel these characteristic features are somehow related to each other. However this problem needs especial investigation that is beyond the scope of the present study.

We thank V.V.Anisovich, L.G.Dakhno, V.A.Nikonov and A.V.Sarantsev for numerous discussions and useful remarks.

Appendix A

Here the G-function parameters are displayed which are obtained by fitting phases and inelasticities of the considered waves. The phase volumes are also presented which are used in the fitting procedure. For the deuteron waves $^3S_1$ and $^3D_1$ the parameters are given in [43].

The simplest way to find the G-functions is provided by (2.22). The N-functions which contain left-hand singularities related to the t-channel meson exchange have the meaning of a potential of the free–nucleon interaction. Because of that, they may change sign. This fact has been taken into consideration by introducing two functions G_1 and G_2, which are determined as follows:

$$N = G_1 G^1 - G_2 G^2. \tag{A.1}$$

In the case when inelasticity appears, the N-function takes a matrix form, namely,

$$\begin{pmatrix} N_{NN\to NN} & N_{NN\to N\Delta} \\ N_{N\Delta\to NN} & N_{N\Delta\to N\Delta} \end{pmatrix}, \tag{A.2}$$

the change of sign is allowed for $N_{NN\to NN}$ only.

By fitting the phase shift data, the following circumstance have been taken into consideration. In eqs. (2.45) and (2.49) the S- and B-matrices depend on the product of functions G and ρ: $G_i\rho_j G^k$. For the NN-scattering without inelasticity, ρ_j is defined by (2.7): $\rho_j = 1/16\pi\sqrt{(s-4m^2)/s} \equiv \rho_0$. But for practical use the phase volume factor ρ_j may be taken in such a way that, on the one hand, it reflects kinematics of the chosen wave and, on the other, it does not violate the convergence of the integral (2.49). Let us introduce auxilliary functions $\rho_j^{(aux)}$ and $G_i^{(aux)}$ which are related to ρ_j and G_i as follows:

$$G_i^{(aux)}\rho_j^{(aux)}G^{k(aux)} = G_i\rho_0 G^k \tag{A.3}$$

Then $G_i = G_i^{(aux)}(\rho_j^{(aux)}/\rho_0)^{1/2}$. In the calculations the functions $G_i^{(aux)}$ (not G_i) were parametrized as follows (2.39): $G_i^{(aux)} = \sum_{n=1}^{N}\gamma_n^i/(s-s_n^i)$. The introduction of $\rho^{(aux)}$ is especially suitable for the waves with inelasticities, when one needs to include the inelastic threshold into the phase space.

Now consider the partial waves. For the waves $^1P_1$ and $^3D_2$ we use the following expressions for $\rho^{(aux)}$:

$$^1P_1: \qquad \rho_{^1P_1}^{(aux)} = \frac{1}{16\pi}\frac{s-4m^2}{\sqrt{s}} \tag{A.4}$$

$$^3D_2: \qquad \rho_{^3D_2}^{(aux)} = \frac{1}{16\pi}\frac{(s-4m^2)^2}{s^2\sqrt{s}}. \tag{A.5}$$

Parameters $G_i^{(aux)}$ are given in Table 1 (for the sake of brevity in Table $G_i^{(aux)}$ is denoted as G_i).

The next step is to include the (πN) resonances into consideration. The modified way of finding out parameters is as follows. First, let the resonance width be zero: $\Gamma_R^w =$

Table 1. G-function parameters for different waves

		γ_1	γ_2	γ_3	γ_4	γ_5	γ_6	s_0	h_0
$^1P_1$	G_1	-.164·10^0	.112 · 10^3	-.568·10^3	.762 · 10^3	.-320·10^2	.-289·10^3	.341 · 10^1	.282 · 10^0
	G_2	.880 · 10^1	-.104·10^3	.204 · 10^3	-.214 · 10^2	-.309·10^1	-.805·10^2	.349 · 10^1	.170 · 10^0
$^3D_2$	G_1	.653 · 10^2	-.368·10^3	.866 · 10^3	.224 · 10^3	.-887·10^3	.-855·10^1	.347 · 10^1	.453 · 10^0
	G_2	-.934·10^1	.465 · 10^3	-.134·10^4	-.209·10^3	.132 · 10^4	.577 · 10^2	.351 · 10^1	.392 · 10^0
	G_1	.320 · 10^4	-.583·10^4	.204 · 10^4	.601 · 10^3	0.0	0.0	.343 · 10^1	.671 · 10^{-3}
	G_2	.499 · 10^2	-.440·10^2	-.107·10^2	-.618·10^1	0.0	0.0	.340 · 10^1	.638 · 10^{-1}
$^1S_0$	G_t	.944 · 10^5	-.100·10^5	-.351·10^3	.327 · 10^4	.996 · 10^4	-.515·10^2	.690 · 10^0	.782 · 10^{-1}
	G_r	-.549·10^3	.616 · 10^3	.919 · 10^3	-.967·10^3	-.241·10^2	-.142·10^1	.390 · 10^1	.666 · 10^{-1}
	G_R	.178 · 10^3	-.205·10^3	-.179·10^1	-.234·10^2	-.192·10^1	-.234·10^2	.406 · 10^1	.864 · 10^{-1}
	G_1	.456 · 10^4	-.817·10^4	.244 · 10^4	.121 · 10^4	0.0	0.0	.329 · 10^1	.100 · 10^{-3}
	G_2	.361 · 10^3	-.399·10^3	-.223·10^2	.156 · 10^2	0.0	0.0	.245 · 10^1	.630 · 10^{-1}
$^3P_0$	G_t	-.554·10^4	.613 · 10^4	-.153·10^5	.441 · 10^3	.128 · 10^5	.952 · 10^3	-.872·10^{-3}	.604 · 10^{-1}
	G_r	-.181·10^3	.500 · 10^1	.860 · 10^3	-.686·10^3	.701 · 10^2	-.172·10^1	.397 · 10^1	.515 · 10^{-1}
	G_R	-.996·10^4	.852 · 10^4	.463 · 10^5	-.679·10^5	.766 · 10^4	.146 · 10^5	.405 · 10^2	.826 · 10^{-2}
	G_1	-.250·10^3	.110 · 10^4	-.207·10^4	.120 · 10^4	0.0	0.0	.334 · 10^1	.133 · 10^0
	G_2	.145 · 10^3	-.112·10^3	-.401·10^1	.843 · 10^1	0.0	0.0	.338 · 10^1	.511 · 10^{-1}
$^3P_1$	G_t	-.190·10^7	.271 · 10^7	-.156·10^5	.122 · 10^4	.125 · 10^5	.311 · 10^3	.678 · 10^0	.745 · 10^{-1}
	G_r	-.213·10^3	.175 · 10^3	.763 · 10^3	-.859·10^3	.108 · 10^3	.184 · 10^2	.360 · 10^1	.281 · 10^0
	G_R	.325 · 10^3	.230 · 10^3	.357 · 10^2	.223 · 10^3	.181 · 10^3	.214 · 10^3	.125 · 10^0	.107 · 10^0
	G_1	-.203·10^2	-.567·10^2	.604 · 10^1	.597 · 10^2	0.0	0.0	.339 · 10^1	.738 · 10^{-2}
	G_2	-.136·10^2	-.287·10^2	-.318·10^1	.644 · 10^2	0.0	0.0	.341 · 10^1	.213 · 10^0
$^3P_2$	G_t	-.183·10^4	-.173·10^4	.922 · 10^2	.194 · 10^2	.876 · 10^1	-.820·10^1	.128 · 10^1	.108 · 10^0
	G_r	.289 · 10^3	-.112·10^4	.915 · 10^3	.797 · 10^2	-.610·10^2	-.232·10^2	.398 · 10^1	.678 · 10^{-1}
	G_R	.908 · 10^0	.979 · 10^0	-.189·10^1	-.251·10^1	.342 · 10^1	.343 · 10^1	.374 · 10^1	.725 · 10^{-1}
	G_1	.473 · 10^4	-.637·10^4	.133 · 10^4	.255 · 10^3	0.0	0.0	.351 · 10^1	.173 · 10^{-2}
	G_2	.834 · 10^0	-.562·10^2	-.159·10^2	.833 · 10^1	0.0	0.0	.294 · 10^1	.636 · 10^{-1}
$^1D_2$	G_t	-.997·10^4	.863 · 10^4	.145 · 10^4	-.391·10^3	.509 · 10^3	-.314·10^3	.351 · 10^1	.236 · 10^{-2}
	G_r	.802 · 10^2	.134 · 10^3	-.456·10^2	-.470·10^3	-.819·10^2	.361 · 10^3	.227 · 10^1	.383 · 10^0
	G_R	.122 · 10^4	-.386·10^3	-.841·10^2	.137 · 10^3	-.343·10^1	.634 · 10^1	-.917·10^2	.117 · 10^{-3}
	G_1	.825 · 10^4	-.747·10^4	-.105·10^4	.361 · 10^3	0.0	0.0	.217 · 10^1	.444 · 10^{-1}
	G_2	.723 · 10^2	-.135·10^3	-.149·10^2	-.736·10^2	0.0	0.0	.335 · 10^1	.106 · 10^0
$^3F_3$	G_t	-.454·10^5	.194·10^5	.151 · 10^5	.275·10^4	.694 · 10^4	-.108·10^4	-.167·10^1	.937 · 10^{-2}
	G_r	-.656·10^3	.155·10^2	.241 · 10^3	.108·10^3	.356 · 10^3	.862 · 10^1	-.231·10^1	.334 · 10^0
	G_Δ	.227 · 10^5	-.135·10^5	-.376·10^4	-.575·10^4	-.393·10^4	-.554·10^2	-.123·10^3	.632 · 10^0

0, where R is one of Δ, N^* or $(\pi N)_S$. Then the phase space factor, for instance, ρ_0^Δ for the isobar related to the loop shown in Fig. 4b, is equal to

$$\rho_0^\Delta = \int d\Phi_{\Delta N} = \frac{1}{16\pi}\sqrt{\frac{(s-(m_N+m_\Delta)^2)(s-(m_N-m_\Delta)^2)}{s^2}}. \quad \text{(A.6)}$$

The trace of the loop of Fig. 4b with the partial operators $O^\kappa_{a,\alpha\beta}$ in the vertices is equal to:

$$Sp\left[O^\kappa_{a,\alpha\beta}P^{\kappa\kappa'}(-p_1+M_R)O^\kappa_{b,\alpha'\beta'}(p_2+m_N)\right] = \delta_{ab}T_{\alpha\beta\alpha'\beta'}\rho_a(s). \quad \text{(A.7)}$$

Here $O^\kappa_{a,\alpha\beta}$ is partial operator which is defined by formulae (2.42), (2.50) and (2.53), without normalizing factor $1/\sqrt{\Omega_a}$. $P^{\kappa\kappa'}$ is given in (3.42).

Consider now the real resonance, with $\Gamma^w_R \neq 0$, decaying into meson and nucleon, and instead of the diagram of Fig. 4b we use that of Fig. 4d. There are three mass-on-shell particles in the intermediate state, that leads to the integral over the resonance mass for the phase volume, together with the normalization factor $\rho_a(s)$ written in (A.7). Then the phase volume for the partial state a has the form:

$$\rho_{\Delta,a} = \int\limits_{(m_n+m_\pi)^2}^{(\sqrt{s}-m_N)^2} d\tilde{s}\frac{1}{16\pi} \times \sqrt{\frac{(s-(m_N+\sqrt{\tilde{s}})^2)(s-(m_N-\sqrt{\tilde{s}})^2)}{s^2}}R(\tilde{s})\rho_a(\tilde{s}), \quad \text{(A.8)}$$

and

$$R(\tilde{s}) = \frac{\Gamma_R^w M_R}{(\tilde{s} - M_R^2)^2 + (\Gamma_R^w M_R)^2}. \quad \text{(A.9)}$$

Normalizing factors in (2.42), (2.50) and (2.53) are equal

$$\Omega_a = \rho_{\Delta,a}$$

Now let us derive the equation (A.8), with the three–particle phase space factor related to the diagram of Fig. 4d. It has the form:

$$\begin{aligned} d\Phi_3 = {} & \frac{1}{2}\frac{d^4k_1}{(2\pi)^3}\delta\left(k_1^2 - m_1^2\right)\frac{d^4k_2}{(2\pi)^3}\delta\left(k_2^2 - m_2^2\right) \\ & \times \frac{d^4k_3}{(2\pi)^3}\delta\left(k_3^2 - m_3^2\right) \\ & \times (2\pi)^4\delta(P - k_1 - k_2 - k_3)\int d^4k_{12}\delta^4(k_{12} - k_1 - k_2) \\ & \times \int dm_{12}\delta\left(P - k_1 - k_2 - k_3\right). \end{aligned} \quad \text{(A.10)}$$

After multiplying it by the unity,

$$\int d^4k_{12}\delta^4(k_{12} - k_1 - k_2)\int dm_{12}\delta(k_{12} - m_{12}), \quad \text{(A.11)}$$

we get the product of two two–particle phase volumes:

$$\begin{aligned} d\Phi_3 = {} & \int \frac{dm_{12}}{\pi}\,\frac{1}{2}\,\frac{d^4k_1}{(2\pi)^3}\,\delta\left(k_1^2 - m_1^2\right)\,\frac{d^4k_2}{(2\pi)^3} \\ & \times \delta\left(k_2^2 - m_2^2\right)\,(2\pi)^4\,\delta^4(k_{12} - k_1 - k_2) \\ & \times \frac{1}{2}\,\frac{d^4k_{12}}{(2\pi)^3}\,\delta\left(k_{12}^2 - m_{12}^2\right)\,\frac{d^4k_3}{(2\pi)^3} \\ & \times \delta\left(k_3^2 - m_3^2\right)(2\pi)^4\delta^4(P - k_3 - k_4). \end{aligned} \quad \text{(A.12)}$$

They are equal to $(m_1 = m_\pi, m_2 = m_N, m_3 = m_N)$:

$$\begin{aligned} & \frac{1}{2}\frac{d^4k_1}{(2\pi)^3}\delta\left(k_1^2 - m_1^2\right)\frac{d^4k_2}{(2\pi)^3}\delta\left(k_2^2 - m_2^2\right)(2\pi)^4\delta^4(k_{12} - k_1 - k_2) \\ & = \frac{1}{8\pi\sqrt{m_{12}^2}}k_{\pi N}\frac{d\Omega_{\pi N}}{4\pi} \\ & = \frac{1}{8\pi\sqrt{m_{12}^2}}\sqrt{\frac{(s - (m_N + m_\pi)^2)(s - (m_N - m_\pi)^2)}{4s}} \\ & \quad \times \frac{d\Omega_{\pi N}}{4\pi}, \\ & \frac{1}{2}\frac{d^4k_{12}}{(2\pi)^3}\delta\left(k_{12}^2 - m_{12}^2\right)\frac{d^4k_3}{(2\pi)^3}\delta\left(k_3^2 - m_3^2\right)(2\pi)^4 \\ & \quad \times \delta^4(P - k_3 - k_4) \\ & = \frac{1}{8\pi\sqrt{s}}k_{N\Delta}\frac{d\Omega_{N\Delta}}{4\pi} \\ & = \frac{1}{8\pi\sqrt{s}}\sqrt{\frac{(s - (m_N + m_{12})^2)(s - (m_N - m_{12})^2)}{4s}} \\ & \quad \times \frac{d\Omega_{N\Delta}}{4\pi}. \end{aligned} \quad \text{(A.13)}$$

Then, one has for the three-particle phase space factor:

$$d\Phi_3 = \int \frac{dm_{12}}{\pi}\cdot\frac{1}{8\pi\sqrt{m_{12}^2}}k_{\pi N}\frac{d\Omega_{N\Delta}}{4\pi}\frac{d\Omega_{\pi N}}{4\pi}. \quad \text{(A.14)}$$

The phase space for the loop diagram of Fig. 4d is

$$\rho_{\Delta,a} = \int d\Phi_3 \frac{\alpha^2}{(m_{12}^2 - m_\Delta^2)^2 + (\Gamma_\Delta^w m_\Delta)^2}\rho_a(s, m_{12}). \quad \text{(A.15)}$$

Here ρ_a is given by (A.7). Then

$$\begin{aligned} \rho_{\Delta,a} = {} & \int\limits_{(m_N+m_\pi)^2}^{(\sqrt{s}-m_N)^2} \frac{dm_{12}}{\pi}\,\frac{k_{\pi N}}{8\pi\sqrt{m_{12}^2}}\,\frac{k_{N\Delta}}{8\pi\sqrt{s}} \\ & \times \frac{\alpha^2}{(m_{12}^2 - m_\Delta^2)^2 + (\Gamma_\Delta^w m_\Delta)^2}\rho_a\frac{d\Omega_{N\Delta}}{4\pi}\frac{d\Omega_{\pi N}}{4\pi}. \end{aligned} \quad \text{(A.16)}$$

The parameter α may be found, using boundary condition $\rho_\Delta \to k_{N\Delta}/(8\pi\sqrt{s})$ at $\Gamma^w \to 0$, providing

$$\alpha = \frac{16\pi\Gamma_\Delta^w m_\Delta^3}{\sqrt{(m_\Delta^2 - (m_N + m_\pi)^2)(m_\Delta^2 - (m_N - m_\pi)^2)}}. \quad \text{(A.17)}$$

Coming back to (A.3), one can find $G = G^{aux}(\rho_\Delta^{aux}/\rho_\Delta)^{1/2}$ for any wave a. However, in this case the triangle diagram $\tilde{\Delta}^i_{\tau\mu\alpha\beta}$ (3.41) should be calculated with non-normalized operators $O^\kappa_{a,\alpha\beta}$, for the normalizing factor has been already included into $(\rho_\Delta^{aux}/\rho_\Delta)^{1/2}$. Comparing (A.8) with (3.43) and (3.44) for $\tilde{\Delta}^i_{\tau\mu\alpha\beta}$, one may see that the Lehman expansion takes explicitly into account the resonance widths, when calculating the graphs 1c,e,f.

In our calculations the following parametrization of the phase space factors is used for the waves $^1D_2$, $^3P_2$ and $^3F_3$:

$$\begin{aligned} {}^1D_2:\ \rho_\Delta^{aux} = {} & \frac{1}{16\pi}\left(0.2\frac{\sqrt{s - (2m_N + m_\pi)^2}}{s}\right. \\ & \left. + 20.0\frac{(s - (2m_N + 0.7m_\pi)^2)^{1/4}}{s^3}\right), \\ \rho_N^{aux} = {} & \frac{1}{16\pi}\frac{\sqrt{(s - 4m^2)^7}}{s^3}, \end{aligned} \quad \text{(A.18)}$$

$$\begin{aligned} {}^3P_2:\ \rho_\Delta^{aux} = {} & \frac{1}{16\pi}\left(0.4\frac{\sqrt{(s - (2m_N + m_\pi)^2)^3}}{s^2}\right. \\ & \left. + 0.3\frac{s - (2m_N + 1.8m_\pi)^2}{s^2}\right), \\ \rho_N^{aux} = {} & \frac{1}{16\pi}\frac{\sqrt{(s - 4m^2)^3}}{s^2}, \end{aligned} \quad \text{(A.19)}$$

$$
{}^3F_3:\ \rho_{\Delta}^{aux} = \frac{1}{16\pi}\left(0.35\frac{(s-(2m_N+m_\pi)^2)}{s^2} + 0.95\frac{s-(2m_N+2m_\pi)^2}{s^2}\right),
$$
$$
\rho_N^{aux}(s) = \frac{1}{16\pi}\frac{\sqrt{(s-4m^2)^5}}{s^3}. \qquad \text{(A.20)}
$$

For the waves ${}^1S_0$, ${}^3P_0$ and ${}^3P_1$ the phase volumes (ρ_R^{aux}) are related to (A.8) as $\rho_R^{aux}(s) = \rho_{\Delta}(s)/s^3$, and $R(\tilde{s})$ is chosen as follows:

$$
R(\tilde{s}) = \sum_{i=1}^{10}\frac{\Gamma_i^w m_i}{(\tilde{s}-m_i^2)^2+(\Gamma_i^w m_i)^2},
$$
$$
m_i = 4.05 + (i-1)0.1. \qquad \text{(A.21)}
$$

The meaning of such a definition of R is connected with an unclear inelasticity nature in the waves ${}^1S_0$, ${}^3P_0$ and ${}^3P_1$. When fitting phase space data, we used as a model for inelasticity the set of 10 resonances with masses m_i and large widths Γ_i^w, these widths defined by the decay vertices to nucleon and meson, c_{π_i}: $c_{\pi_i} = 0.028 + (i-1)0.028$, and

$$
\Gamma_i^w = \frac{1}{16\pi m_i^2}c_{\pi,i}^2\left((m_i+m_N)^2-m_\pi^2\right) \qquad \text{(A.22)}
$$
$$
\times\sqrt{\frac{(m_i^2-(m_N+m_\pi)^2)(m_i^2-(m_N-m_\pi)^2)}{m_i}}.
$$

The derivation of this formula is similar to that of Sect. 2.3. Parameters of $G^{(aux)}$ are presented in Table 1 (in Table 1 $G_i^{(aux)}$ is denoted as G_i).

For the wave ${}^1S_0$, several inelasticity variants are considered. To get vertices G_i which respond to $\Delta(1232)$, N^* or $(\pi N)_S$, one should correctly calculate the phase spaces ρ_{Δ}, ρ_{N^*} or $\rho_{(N\pi)_S}$ using (A.7) and (A.8), with the mass M_R and width Γ_R^w related to considered variant. Then the G-functions are calculated using (A.3).

References

1. R. Moreh, T.J. Kennett, and W.V. Prestwich: Phys. Rev. **C39** (1989) 1247
2. Y. Birenbaum, S. Kahane, R. Moreh: Phys. Rev. **C32** (1985) 1825
3. R. Bernabei, A. Incicehitti, M. Mattioli, et al: Phys. Rev. Lett. **57** (1986) 1542
4. E. De Sanctis, M. Anghinolfi, G.P. Capitani, et al: Phys. Rev. **C34** (1986) 413
5. J. Arends, H.J. Hassen, A. Hegerathet, et al: Nucl. Phys. **A412** (1981) 509
6. , T. Stiehler, B. Kühn, K. Möller, et al: Phys. Lett. **B151** (1985) 185
7. J. Ahrens, H.B. Eppler, H. Gimm, et al: Phys. Lett. **B52** (1974) 49
8. J.M. Cameron: Can. J. Phys. **62** (1984) 1019.
9. A. Zieger, P. Crewer, and B. Ziegler: Phys. Lett. **B285** (1992) 1
10. M.P. Pascale, G. Giordano, G. Matone, et al: Phys. Rev., **C32** (1985) 1830
11. D.M.Shopik, Y.M. Shin, M.C. Phenneger, et al: Phys. Rev. **C9** (1974) 531
12. P. Levi Sandry, M. Anghinolfi, N. Bianchi, et al: Phys. Rev. **C39** (1989) 1701
13. H.O. Meyer, J.R. Hall, M.Hugi, et al: Phys. Rev. **C31** (1985) 309; H.O. Meyer, J.R. Hall, M.Hugi, et al: Phys. Rev. Lett. **52** (1984) 1759
14. G.F. Chew and S. Mandelstam: Phys. Rev. **119** (1960) 467; G.F. Chew: "The analytic S-matrix". W.A. Benjamin, Inc. New-York — Amsterdam, 1966
15. F.E. Close: *private communication*; N. Isgur: "Spin structure of the proton: a quark modeler's view", JLAB-THY-96-14, 1996
16. V.V.Anisovich, D.I Melikhov, and V.A.Nikonov: Phys. Rev. **D52** (1995) 5295; *ibid* **D55** (1997) 2918
17. R.A. Arndt, J.S. Hyslop III, L.D. Roper: Phys. Rev. **D50** (1987) 128
18. V.V. Anisovich, E.P. Kistenev, and M.N. Kobrinsky: Sov. J. of Nucl. Phys. **14** (1971) 441
19. G. Veneziano: Nuovo Cim. **A57** (1968) 190.
20. F. Gross: Phys. Rev. **140B** (1965) 410; G.B. West: Ann. Phys. **74** (1972) 464
21. V.V. Anisovich, M.N. Kobrinsky, D.I. Melikhov, and A.V. Sarantsev, Nucl. Phys. **A544** (1992) 747
22. S. Mandelstam: Phys. Rev. Lett. **4** (1960) 84; R. Blankenbecler and Y.Nambu: Nuovo Cim. **18** (1960) 595; R. Blankenbecler and L.F.Cook: Phys. Rev. **119** (1960) 1745; R.E. Cutkosky: Rev. Mod. Phys. **33** (1961) 448
23. V.V. Anisovich, D.I. Melikhov, B.Ch.Metch, and H.R.Petry: Nucl. Phys. **A563** (1993) 549
24. F. Gross, J.W. Van Orden, and K. Holinde, Phys. Rev. **C41** (1990) 1909
25. H. Arenhovel: Ch. J. of Phys. **30** (1992) 17
26. V.A. Karmanov: JETF **71** (1976) 399
27. M.D. Teren'tiev: Yad. Fiz. **24** (1976) 207
28. .I. Kirillov, B.E.Troitsky, S.V.Trubnikov, J.M.Sirkov: Particles and Nuclei **6** (1975) 3
29. L.A. Kondratyuk, and M.I. Strikman: Nucl. Phys. **A426** (1984) 575
30. F. Partovi: Ann. Phys. **27** (1964) 79
31. J.M. Laget: Nucl. Phys. **A312** (1978) 265
32. W. Jaus and W.S. Woolcock: Nucl. Phys. **A473** (1987) 667
33. H. Arenhovel: Nuovo Cim. **A76** (1983) 256; W. Leidemann and H. Arenhovel: Nucl. Phys. **A465** (1987) 573
34. K. Ogawa, K. Kamae, and K. Takamura: Nucl. Phys. **A340** (1980) 451
35. H. Tanabe and K. Ohta: Phys. Rev. **C40** (1989) 1905
36. M. Anastasio and M. Chemtob: Nucl. Phys. **A364** (1981) 219
37. M.I.Levchuk: Few-Body Systems **19** (1995) 77
38. A.V. Anisovich and V.A. Sadovnikova: Sov. J. Nucl. Phys. **55** (1992) 1483; A.V. Anisovich, and V.A. Sadovnikova: Phys. of Atom. Nucl. **57**, 1322 (1994); A.V. Anisovich and V.A. Sadovnikova: Bull. Acad. Sci. Russia **59** (1995) 151; A.V. Anisovich and V.A. Sadovnikova: Phys. of Atom. Nucl. **59** (1996) 616
39. M. Fierz: Zeit. Phys. **104** (1937) 553
40. L. Castillejo, R. Dalitz, F. Dyson: Phys. Rev. **101** (1956) 453

41. V.V.Anisovich, D.V.Bugg, and A.V.Sarantsev: Nucl. Phys. **A537** (1992) 501
42. D.V. Bugg : Proc.of the 3th Int. Symp. on πN and NN physics, 1989, Gatchina, p.57; R. Dubois, D. Axen, R. Keeler, et al: Nucl. Phys. **A377** (1982) 554; W.M. Kloet and J.A. Tjon: Phys. Lett. **B106** (1981) 24; D.V. Bugg, A. Hasan, and R.L.Shypit: Nucl. Phys. **A477** (1988) 546
43. A.V. Sarantsev: "Quantum Inversion Theory and Applications", in *Lecture Notes in Physics*, ed. H.V. Geramb, 1993, p. 465
44. R.A. Arndt, L.D. Roper, R.A. Bryan et al: Phys. Rev. **D28** (1983) 97
45. M. Gourdin and Ph. Salin: Nuovo Cim. **27**, (1963) 193
46. Particle Data Group: Phys. Rev. D**54** (1996) 601
47. T.A. Armstrong, W.R.Hogg et al.: Nucl.Phys. **B41** (1972) 445
48. G.P. Lepage and S.J. Brodsky: Phys. Rev. **D22** (1980) 2157
49. L. Frankfurt and M. Strikman: Phys. Report **C76** (1981) 215